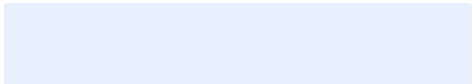## University of Stavanger

Faculty of Science and Technology

MASTER THESIS

Study Program/Specialization: Petroleum Engineering Reservoir Engineering	Spring Semester, 2020 Open
Author: Armin Shahab	.... (author signature)

Faculty Supervisor(s):Dhruvit Satishchandra Berawala, Pål Østebø Andersen

Master thesis title: CO_2 Injection in Shales for CCUS

Credits(ECTS) :30

Keywords: Shale Gas Reservoirs Co_2 Injection	Number of pages: 45 + appendices/other: 3 Stavanger, 15/08/2020 date/year

Acknowledgement

Table of Contents

List of Figures

List of Tables

Nomenclature
Roman
a_i	=	Adsorbed component, mol / m3 rock
$\hat{a}_i$	=	Adsorbed component, Pa
A	=	Specific surface area, m2 / m3 rock
A_i	=	Adsorbed specific surface area by component, m2 / m3 rock
b_g	=	Inverse gas volume factor, m3 gas at standard conditions / m3 gas at reservoir conditions
b_g'	=	Inverse gas volume factor differentiated with respect to total pressure, Pa-1
B_i	=	Coefficient to relate $\hat{a}_i$ and A_i, Pa m3 rock / m2
C_i	=	Component molar concentration, mol / m3 gas
D_i	=	Diffusion coefficient, m2/s
K_a	=	Apparent permeability, m2
K_i	=	Equilibrium constants for adsorption of component i, Pa^{n_i}
K_n	=	Knudsen number, dimensionless
L	=	System length, m
M_i	=	Conservation variable for each component, Pa
$M_{w,i}$	=	Molar weight gas component, kg / mol
$M_{w,g}$	=	Molar weight gas, kg / mol
n_i	=	Ratio of moles of component adsorbed in multilayer mode to monolayer mode, dimensionless
N_i	=	# moles of component, mol
N_t	=	# moles of gas, mol
P_i	=	Partial pressure of component, Pa
P_t	=	Total pressure, Pa
r	=	Pore radius, m
R	=	Gas constant, J / mol
RF	=	Methane recovery factor, dimensionless
$S_{m,i}$	=	Moles that adsorb per area during monolayer adsorption at full capacity, mol / m2
T	=	Absolute temperature, K
u	=	Gas flux, m/s
V_g	=	Gas volume, m3
W_i	=	Adsorbed mass of component per volume dry rock, kg / m3 rock
x	=	Spatial coordinate, m
x_i	=	Mole fraction, dimensionless
z	=	Real gas deviation factor, dimensionless

Greek
Ψ_m	=	Matrix permeability-stress-dependence factor, Pa-1
σ_m'	=	Mean effective stress, Pa
η_m	=	Matrix porosity-stress-dependence factor, Pa-1
α_K	=	Rarefraction parameter, dimensionless
μ_g	=	Gas viscosity, Pa s
ρ_g	=	Gas molar density, mol / m3 gas
$\rho_{g,sc}$	=	Surface gas molar density, mol / m3 gas
τ	=	Tortuosity, dimensionless
ϕ	=	Porosity, dimensionless

Indices
base	=	Under pressure depletion condition

c	=	Carbon dioxide CO_2
f	=	Fracture
i	=	Component;
init	=	Initial conditions
inj	=	Under CO_2 injection conditions
m	=	Methane CH_4
sc	=	Surface conditions
well	=	Well conditions

Abbreviations

EGR	=	Enhanced gas recovery
GOIP	=	Gas originally in place
GCIP	=	Gas currently in place

1. Introduction :

1.1. Shale Gas – Geology and general overview

Shale gas is produced in the high organic shale formations that formerly considered as caprock or source rock but nowadays typically function as a reservoir rock for natural gas. With regard to the chemical components about 90 percent or more is methane so typically is a dry gas but, in some formations, produces wet gas (Boyer et al.2006). Shale is a consolidated sedimentary rock with fine-grained clay particles. In low-energy depositional environments such as deep-water basins, shale precipitated as mud type due to the quiet water. Also in the company of shale, there are organic matters in the form of algae-, plant-, and animals-derived organic sediments (Davis, 1992). Clay grains are naturally tabular and tend to lie flat when the sediments are deposited and consequently compacted as a result of overburden pressure. Tabular grains of clay during petrification make a thin layer with limited horizontal permeability and extremely low vertical permeability. The common unfractured shale matrix permeability is on the order of 0.01 to 0.00001 millidarcy (Freeze & Cherry, 1979). This amount of permeability in shale means the gas that is trapped in the pores could not move outside except during geological times (millions of years). The low permeability properties of shale cause to be classified as an unconventional reservoir. (Nuttall & Daugherty, 2012). Gas reservoirs are classified into conventional and unconventional. In conventional reservoirs gas produced from sands and carbonates (dolomite and limestones) that contain gas in interconnected pore space that flows to the wellbore. This kind of reservoirs is like a kitchen sponge in which gas can move from one pore to another pore through the smaller pore-throats that make a permeable flow in the reservoir (Nash, 2010, page .20). However in unconventional reservoirs gas produced from low permeable (tight) reservoir rocks such as tight sands and carbonates, coal, and shale. Because of low permeable rock types in unconventional reservoirs, for a cost-effective production we need combination of a hydraulic fracturing and horizontal drilling. So there will be opportunities in the economic production of gas in regard to world demand energy.

1.2. Key Role of Shale Gas in the Future

With progress in the oil and gas industry, horizontal drilling and hydraulic fracturing would be a reasonable choice for the development of unconventional reservoirs especially shale gas as the main source of natural gas for domestic and world demand. In spite of complex geological and petrophysical systems of shale gas, there will be huge potential for future reserve growth and production (Newsham & Rushing, 2001). In the future, unconventional gas resources will be the main supply of global energy due to the fast decline of conventional reserves, the huge quantity and extensive distribution of tight reservoirs (Hai Sun, Yao, Cao, Fan, & Zhang, 2017). Shale gas revolutionized the gas industry in the US and global markets. Shale gas resources estimated at around 7,300 Tcf by Energy Information Administration (EIA) and globally, 32% of the total estimated natural gas are in shale formations. The US only has 665

Tcf of technically recoverable shale gas resources (*Annual Energy Outlook 2013 - EIA*, n.d.; Hao Sun, Chawathe, Hoteit, Shi, & Li, 2015). As it is shown in Figure 1-1 the volume of unconventional gas reservoirs is more than conventional gas reservoirs. But unconventional development needs more advance technology and money.
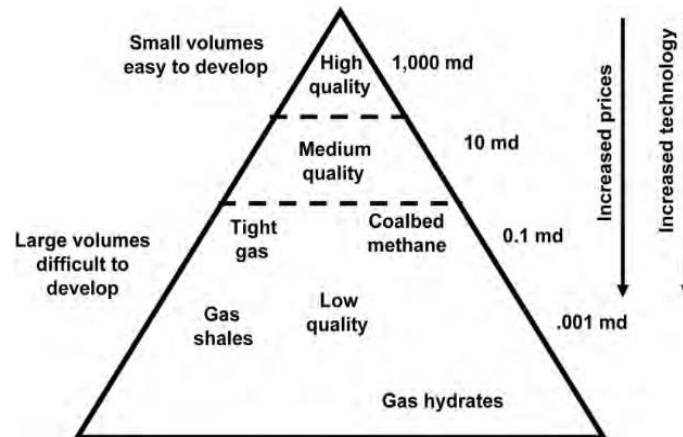
Figure 1-1 Resource triangle for gas

(Lake, Fanchi, & Society of Petroleum Engineers (U.S.), 2006)

1.3. Shale Gas Features

Shale gas reservoirs are made up of fine clay grains with small pore sizes ranging from micrometer to nanometers. Almost three different permeability exists in shale rocks, one is the permeability of matrix texture, natural fractures and hydraulic fractures after stimulation. But the range of highly low-permeability rocks for being more economically viable in many unconventional gas reservoirs is 10 to 100 nano-Darcy. A common shale gas reservoir demonstrates a net thickness of 50 to 600 ft, the porosity of 2 to 8 %, and total organic carbon of 1 to 14 % is explored at depths ranging from 1000 to 13000 ft. Natural gas will be stored in shale gas reservoir in one three forms: (1) free gas in pores and fractures, (2) adsorbed gas in organic matter and on inorganic minerals, and (3) as a dissolved gas in oil and water (T. Zhang, Ellis, Ruppel, Milliken, & Yang, 2012). A huge amount (20-85 %) of methane stored as an adsorbed form (Hill & Nelson, 2000), and just a small portion of it will be produced during the production life of a shale gas well (Cipolla, Lolon, Erdle, & Rubin, 2010). After a few years of production from a shale gas well, there will be a rapidly pressure depression that causes the estimated ultimate recovery is rarely constrained during the early stages of field development and is the main reason why the development of shale gas is economically risky (Weijermars, 2013). However, interest in enhanced shale gas recovery has grown in recent years (Kim, Cho, & Lee, 2017).

1.4. Production of Shale Gas

Due to the development of hydraulic fracturing and horizontal drilling, there has been immense progress in natural gas production from tight formations. Nonetheless, the gas recovery ratio is infinitesimal from these reservoirs. Gas flow as we mentioned in the past involving several

complicated processes that coupled with each other and affect the production and ultimate gas recovery. Hydraulic stimulation is a crucial stage in creating and maintaining a high permeability path. So, it will be introduced by a slurry of surfactants, corrosives, and small ceramic particles. For prevention of fracture closure, after stimulation and during pressure depletion, small ceramic particles will remain between fracture and keep them open during the life of the well (Hellmann, Scheetz, Luscher, Hartwich, & Koseski, 2014).

1.5. Simulation of Shale Gas Reservoirs

For the prediction of shale gas reservoir production, there is a necessity to use commercial reservoir simulators but due to complications of shale gas reservoir flow regimes, some parameters are overestimated or underestimated. As an example, the volume that occupied by adsorbed layer is neglected, so the volume of free gas overestimated. In addition, stress dependency of matrix and surface diffusion in shale gas layers is excluded from commercial simulators (J. Wang et al., 2017). For counting of the gas original in place (GOIP) in shale reservoirs, we need more accurate in-depth models to develop for lab studies and further in field applications.

1.6. Enhanced Gas Recovery and CO2 Sequestration

On the base of facts and figures, CO_2 storage during CO_2-EOR in conventional reservoirs is an efficient method and the possibility for sequestration in unconventional oil and gas reservoirs is more promising and economically beneficial, but yet there is minimum consideration about this tremendous resources of energy (Sherifa & Reza, 2018). In organic-rich shale gas and coal seams, the methane adsorbed on kerogen and clay mineral surfaces and also free methane exist in fracture porosity, intergranular micro-porosity and micro-pores in the kerogen. In coal seams and shale gas showed that CO_2 can be preferentially adsorbed relative to methane. A schematic view of the adsorption and desorption procedure is shown in Figure 1-2. In addition, some portion of the pore volume that contains free gas is expected to be available for CO_2 storage (Godec, Koperna, Petrusak, & Oudinot, 2014).
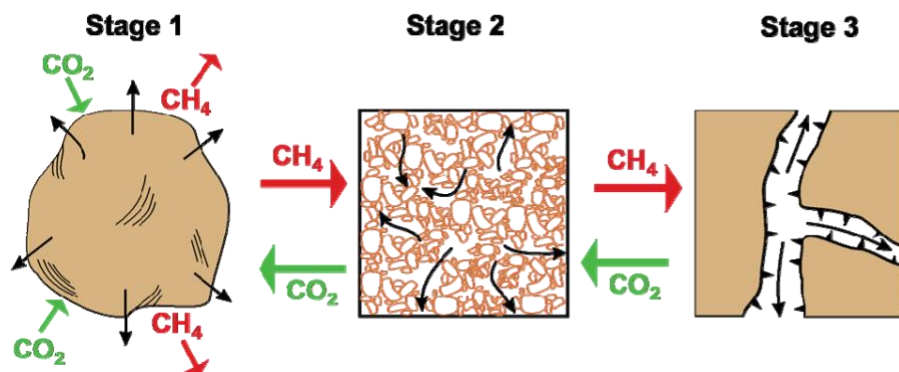

Figure 1-2 Schematic of the flow dynamics of CO2 and CH4 in shale gas

(GODEC ET AL. 2014)

Reliable data in adsorption that measured at reservoir conditions and authentic adsorption model are two crucial specifications in describing shale behavior in gas adsorption. Until now we have a limited amount of data about high-pressure gas adsorption but our data is true for CO_2 adsorption at higher pressures. On the base of experiments, it seems that adsorption capacities of CO_2 or CH_4 related to total organic carbon (TOC) content of shales (Busch et al., 2008; Charoensuppanimit, Mohammad, & Gasem, 2016; Heller & Zoback, 2014; Weniger, Kalkreuth, Busch, & Krooss, 2010). As well, when there is a mixture of CO_2 and CH_4, carbon dioxide adsorbs over methane (Billemont, Coasne, & De Weireld, 2013; Dreisbach, Staudt, & Keller, 1999; Edwards, Celia, Bandilla, Doster, & Kanno, 2015; Kurniawan, Bhatia, & Rudolph, 2006; Ottiger, Pini, Storti, & Mazzotti, 2008). The adsorptive surface of kerogen for gas adsorption, nanopores in kerogen and the tendency of kerogen for adsorption of CO_2 over CH_4 could desorb the methane and adsorb more carbon dioxide, also extremely tight-permeability of shale gas rock matrix make it one of the advantageous choices for safe CO_2 capture. So there will be lots of research and demand in CO_2 sequestration in shale gas formations in the close future (Berawala & Østebø Andersen, 2019a). When we consider unconventional resources, most of our focus is on organic shales. Two key parameters differ unconventional from conventional, first the extremely low matrix permeability and second free gas in pores and adsorbed gas on the surface of kerogen (Blasingame, 2008; Moridis, Blasingame, & Freeman, 2010). The gas amount is trapped in pores firmly dependent on organic matter content, clays, and the ability adsorption of methane on the internal surface of solid. It is provided a complete description of flow mechanisms in shale gas by Blasingame and Moridis (Blasingame, 2008; Moridis, Blasingame, & Freeman, 2010), and there are discussions about the importance of adsorption/desorption mechanisms that happen in pore internal layer. Civan (2010) used the Beskok and Karniadakis (1999) model of rarefied for computing of gas flow in microchannels and the definition of gas transport in shales (Ali Beskok, 1999; Civan, 2010). Simulation in shale gas will be more complicated due to severe heterogeneity, Klinkenberg or slippage effects (Klinkenberg, 1941), and interference of geomechanical parameters. One of the complexities in shale gas is the defining of flow and another complicated subject is the modeling of shale gas flow in fractures, its geometry and interactions of fracture/matrix.

1.7. Objective

For the investigation of controlling factors during the production of shale gas reservoirs, a straightforward mathematical 1D+1D model is presented. In this model, a high permeability fracture broadens from a well perforation and is located between an identically ultra-low permeability matrix. This model is the continuation of the previous works by Berawala et al. (2019) and Berawala et al. (2018). In the new contribution, the effect of multicomponent adsorption-desorption in the shale gas matrix with a fixed-shape fracture will be considered. In this model the following questions will be considered: (i) how the multicomponent adsorption-desorption alter the gas recovery in shale gas reservoirs? (ii) how porosity and permeability will be affected by multicomponent adsorption-desorption ? (iii) what is the effect of uniform fracture without compaction effects in gas recovery, and (iv) what are the potential advantages of this model in shale gas recovery?

2. Theory
2.1. Different Mechanisms in Shale Gas Reservoirs

During many years of studies about shale gas reservoir development, there have been lots of formulas for the definition of flow regimes in matrix and fracture. But some of these methods are more functional and realistic. For evaluation of flow in shale gas reservoirs, two parameters are the key points, one is cumulative gas production and the other one is apparent permeability which is almost absolute permeability here for simplification. There will be considered the shale gas reservoir as a dry gas reservoir with no bound water on clays and so there is a single-phase flow. In conventional reservoirs normally Darcy's law more fit with gas flow conditions, however, in shale gas flow, Darcy's law is not enough extensive to include all flow mechanisms (Blasingame, 2008; Moridis et al., 2010). There are two main phenomena that happen in the shale matrix which yield non-Darcy flow, one is gas slippage (Klinkenberg effect) and the other one is Knudsen diffusion. (H. Wang & Marongiu-Porcu, 2015). Also, the gas flow will be impacted by other mechanisms such as gas desorption or adsorption, surface diffusion and geomechanical effects (Y.-S. Wu, Li, Ding, Wang, & Di, 2014). In the rest, we will consider the important mechanisms in shale gas reservoirs.

2.2. Knudsen Diffusion and Apparent Permeability

we know that from before nanopore structure of shale matrix causes Darcy's law not to be more appropriate for computing of fluid flow in shales. So, there will be other forms of flow mechanisms such as slip-flow regime, transition-flow regime, free molecular regimes (Knudsen diffusion) (Berawala, Andersen, & Ursin, 2019). Knudsen diffusion is a kind of diffusion that mostly happens when the gas molecules collision with each other is more frequent than pore walls. The definition of Knudsen number is a dimensionless parameter for the characterization of different flow regimes in nanochannels (H. Wang & Marongiu-Porcu, 2015). The Knudsen number is the ratio of mean free path length λ, over effective pore radius, r_e (Knudsen, 1909):

$$K_n = \frac{\lambda}{r_e} \tag{1}$$

So the mean free path computed by: (Civan, Rai, & Sondergeld, 2011).

$$\lambda = \frac{\mu_g}{P} \sqrt{\frac{\pi R T}{2 M}} \tag{2}$$

where μ_g is the gas viscosity, T is the reservoir temperature, P is the reservoir pressure, M is the gas average molecular weight, and R is the universal gas constant. With encompass of the real- gas Z-factor, which gives: (H. Wang & Marongiu-Porcu, 2015).

$$K_n = \frac{\mu_g Z}{P \, r_e} \sqrt{\frac{\pi R T}{2M}} \tag{3}$$

The apparent permeability of shale gas could be shown by following general form that depends on only the Knudsen number K_n, and the effective inherent permeability $k_{\infty e}$ (Karniadakis, Beşkök, & Aluru, 2005).

$$k_a = k_{\infty e}\, f(k_n) \tag{4}$$

Florence et al. (2007) expanded this formula to characterize the non-Darcy gas flow in shale layers:(Florence, Rushing, Newsham, & Blasingame, 2007).

$$k_a = k_{\infty e}(1 + a_K k_n)\left(1 + \frac{4k_n}{1 + k_n}\right) \tag{5}$$

where a_K is the rarefraction factor:

$$\alpha_K = \frac{128}{15\pi^2}\tan^{-1}(4K_n^{0.4}) \tag{6}$$

With considering the effect of matrix compaction and adsorbed layer on the nanopore geometry, the effective inherent permeability is :(Jiang & Yang, 2018).

$$K_{\infty e} = \frac{r_e^2}{8}\frac{\phi}{\tau} \tag{7}$$

The parameter r_e is the effective radius of the flow path and τ is the tortuosity of rock. Huang and Ghassemi (2015) and Cao et al. (2016) generalized equation that integrates the whole important parameters which are effective stress, adsorption and flow regimes for apparent gas permeability (Berawala et al., 2019; Cao, Liu, & Leong, 2016; Huang & Ghassemi, 2015).

$$k_a = \frac{r_e^2}{8}\frac{\phi}{\tau}(1 + a_K k_n)\left(1 + \frac{4k_n}{1 + k_n}\right) \tag{8}$$
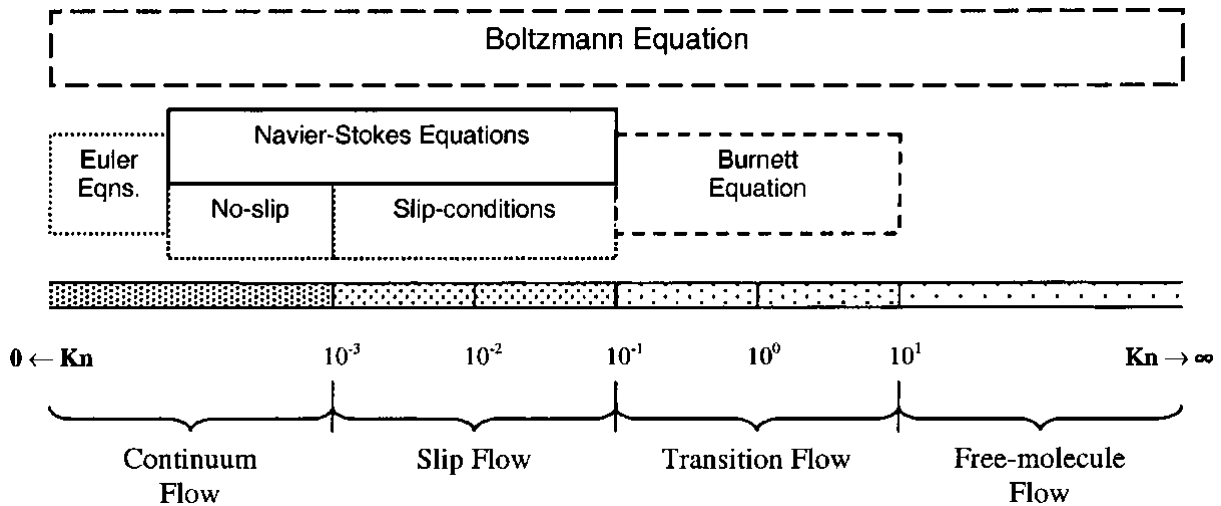
Figure 2-1 classification of gas-flow regimes regarding to Knudsen number.

(Roy, Raju, Chuang, Cruden, & Meyyappan, 2003)

2.3. Transition from Darcy Flow to Non-Darcy Flow

In Darcy's law where there is a continuum flow, the fluid velocity is zero on the pore wall (Sherman, 1969). This is a valid presumption when there is a conventional reservoir and having pore radii between 1 to 100 micrometers that is possible to consider flow as a continuous medium (H. Wang & Marongiu-Porcu, 2015). Due to ultra-tight permeability in shale gas reservoirs, conventional flow rules could not describe gas flow behaviors. The main propulsive force is pressure gradient in pores which cause first free gas move from a matrix to fracture and then wellbore. And second gas is desorbed from kerogen surface and flows. These desorption process is pressure-dependent and is defined by Langmuir's isotherms (Berawala & Østebø Andersen, 2019b). When there is a high flow rate in nanopores near gas production wells or near wellbore regions, particularly in fractures, inertial forces are dominant versus viscous forces (Hagoort, 2004). In (1901) Forchheimer added a term to Darcy's equation to simulate gas flow at high flow rates more accurately (Barree & Conway, 2005; Belhaj et al., 2003; Jones, 1987; Li & Engler, 2001; Ling, He, Wu, & Shen, 2013; Mustapha, de Langavant, & Giddins, 2015; Zeng & Zhao, 2006). A comparison of hydraulically fractured wells with non-fractured wells, hydraulic fractures cause a reduction in the efficiency of non-Darcy flow, it means that normally we expect average flow velocity near the fracture will be dominantly lower than to recompense the high velocities in fracture for the same rate of well production. Nonetheless, near the tip of fracture, there are extremely high local velocities that show the high potential of non-Darcy flows (Hagoort, 2004). Gas transportation is a combination of viscous flow, Knudsen diffusion, and molecular diffusion (Bird, 2002). Also, Javadpour (2009) believes that viscous flow and Knudsen diffusion are the main controlling parameters in gas transport (Javadpour, 2009). In below demonstrate, schematic of viscous flow and Knudsen diffusion from Zobck (Zoback & Kohli, 2019).

Figure 2-2 viscous (continuum) flow vs. Knudsen diffusion. Increased interaction between gas molecules and pore walls at small pore sizes promote diffusive flow mechanisms, resulting in non-zero flow rates along pore walls (slip flow).

(ZOBACK & KOHLI, 2019)

If the mean free path of gas molecules is at least one order of magnitude larger than pore diameter, there is a molecular diffusion (Ho & Webb, 2006). And if mean free path of gas

molecules is much smaller than pore diameter, the possibility of collision between gas molecules is more than the collision of gas with pore walls, so we have viscous flow and Knudsen diffusion can be ignored. By using the Knudsen number, gas transport in porous media will be divided into four flow regimes. Adapted from Zoback (Zoback & Kohli, 2019).

Flow regime	Knudsen number, Kn	Driving force	Model
Continuum (viscous) flow	$Kn < 0.01$	Total pressure gradient	Assumes zero flow velocity along pore walls. No permeability correction required
Slip flow	$0.01 < Kn < 0.1$	Mostly viscous flow with some diffusion	Darcy's law with Klinkenberg correction
Transition flow	$0.1 < Kn < 10$	Mostly diffusion with some viscous flow	Darcy's law with Knudsen correction
Knudsen (molecular) diffusion	$Kn > 10$	Total concentration gradient	Knudsen diffusion equation

Table 2-1 summary of flow regimes as function of Knudsen number.

Adapted from Ziarani and Aguilera (2012) and Heller et al. (2014)

(Heller & Zoback, 2014; Ziarani & Aguilera, 2012).

2.4. The Klinkenberg or Gas Slippage Effect

In shale gas when the pore radii are between 1 to 200 nanometer, so fluid continuum theory does not work and molecules tend to strike against the pore walls and slip on the wall (Sherman, 1969). In 1941 when Klinkenberg was investigating rarefied gas flow at different pressures, he found that the actual gas flow rate is larger than the prediction of Darcy's law. For correction of this deficiency, he proposed apparent permeability that could be adjusted by the slippage parameter (H. Wang & Marongiu-Porcu, 2015). By consideration of Klinkenberg effect, the gas permeability and production will be increased. In (1941) Klinkenberg presented that effective permeability of gas at a finite pressure will be as below:

$$K_g = K_\infty \left(1 + \frac{b}{P} \right) \tag{9}$$

b is the Klinkenberg factor and it is dependent on pore structure and gas temperature and in very large gas pressure is negligible and K_∞ is absolute permeability (Y.-S. Wu, Pruess, & Persoff, 1998).

2.5. Transition Flow

The mechanics of transition flow are sophisticated and most of the models are on the base of Monte Carlo simulation results. The model is applied in different shear stress laws in the Navier-Stokes equation. The below formula indicates the nonlinearity of permeability increase with K_n. For more simplification, derived a polynomial form for permeability raise for

$0.1 < K_n < 0.8$, which is in the range of interest for shale gas reservoirs (Sakhaee-pour & Bryant, 2011).

$$\frac{K_g}{K_l} = 0.8453 + 5.4576\,K_n + 0.1633\,K_n^2 \tag{10}$$

K_g is a single-phase gas permeability, K_l is the permeability of a conduit to liquid with no-slip boundary condition and K_n is the Knudsen number. The above formula coefficient is calculated by using a nonlinear regression model and the regression coefficient is 0.99. It is important that the above formula is just applicable for the transition flow regime also no longer the gas permeability is a linear function of K_n. This means that the Klinkenberg correction could not be applied for the higher Knudsen number flow regime (Sakhaee-pour & Bryant, 2011).

2.6. Molecular Flow (Knudsen Flow)

In this flow regime molecules hit more the pore walls rather than slip. The molecular flow regime is almost unlikely to happen in shale gas reservoirs (K. Wu, Li, Guo, Wang, & Chen, 2016). Knudsen's number in this flow model is more than 10 and the driving force is the total concentration gradient and the model is on the base of the Knudsen diffusion equation (Heller & Zoback, 2014; Ziarani & Aguilera, 2012).

2.7. Surface Diffusion

Surface diffusion is an important transfer mechanism, and its role in gas transportation is inevitable and even under the condition of smaller nanosized pores, this phenomenon will be dominated (Wua, Li, Guo, & Chen, 2015). Free gas transportation in nanopores and surface diffusion are coexistent phenomena in shale gas reservoirs. The adsorbed gas in pore could occupy part of the pore volume cause to reduce free gas transport capacity (Akkutlu & Fathi, 2012). Nonetheless, the adsorbed gas surface diffusion lonely could increase total gas transport capacity in pores. The driving force of surface diffusion is a concentration gradient. Shales with a great specific surface area has adsorbed gas on organic pore walls with a large concentration gradient (Clarkson et al., 2013; Yi, Akkutlu, Karacan, & Clarkson, 2009); accordingly, the surface diffusion is a key point in the transport of gas (Fathi & Akkutlu, 2014; Kang, Fathi, Ambrose, Akkutlu, & Sigal, 2011; Xiong, Devegowda, Michel Villazon, Sigal, & Civan, 2012). In the existence of surface diffusion, the value of apparent permeability could be 10 times that of continuum hydrodynamic (Darcy's method) methods (Darabi, Ettehad, Javadpour, & Sepehrnoori, 2012), even several orders of magnitude more (Holt, 2006; Majumder, Chopra, Andrews, & Hinds, 2005). In Figure 2-3 a schematic diagram of the free gas in nanopores and desorbed gas on nanopore walls is demonstrated.
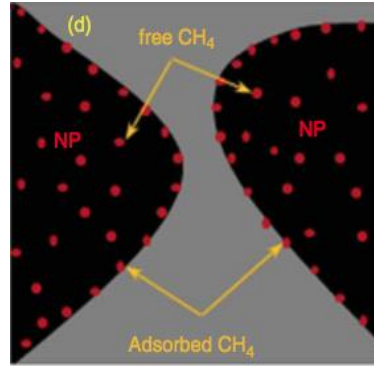
Figure 2-3 gas transport in shale gas , free gas in nanopores and desorbed gas on nanopore walls.

(Ghanbarnezhad Moghanloo & Javadpour, 2014)

2.8.　Adsorption / Desorption

In general, there are two typical models that suit shale gas reservoirs for adsorption and desorption modeling. The Langmuir isotherm (Langmuir, 1918), is used for the description of monolayer gas adsorption on the surfaces but BET isotherm (Brunauer et al. 1938), is for the description of multilayer adsorption. Recently, studies approved the function of BET isotherm in some types of shales (Alnoaimi & Kovscek, 2013; Yu & Sepehrnoori, 2014; Z. Y. Zhang & Yang, 2012). However, the Langmuir isotherm is the most common model in lots of publication to date relevant to shale gas reservoirs (Dong, Holditch, & McVay, 2012; Haghshenas, Clarkson, & Chen, 2013; Lu, Li, & Watson, 1995; Mengal & Wattenbarger, 2011; Shabro, Torres-Verdin, & Javadpour, 2011). An authentic model of isotherm for adsorption/desorption processes is absolutely important because it has a great impact on the gas production rate (J. Wang et al., 2017). Langmuir isotherm demonstrates the amount of adsorbed gas on the solid surface as a function of pressure and constant temperature.

$$V_G = \frac{V_L\, P_g}{P_g + P_L} \tag{11}$$

V_G is the gas content, V_L is the Langmuir volume which demonstrates the maximum storage capacity of gas volume. P_L is Langmuir pressure and P_g is the formation pressure. Under the initial condition of shale gas reservoirs, there is an equilibrium between adsorbed gas and free gas in nanosized pores (Wua et al., 2015). During pressure depletion, adsorbed gases on kerogen convert to free gas and this physical process is very quick (Xiong et al., 2012). Since there is single layer adsorption, the gas coverage of an ideal gas could be formulated as below: (Wua et al., 2015).

$$A_i = A\, \frac{P}{P_L + P} \tag{12}$$

A is a total surface area that available for adsorption, A_i adsorbed specific surface area by component. For a complete adsorption model that cover our multicomponent adsorption, it is needed a comprehensive model that A is the total surface area, A_f is free sites area, A_m is the area occupied by methane and A_c is the area covered by carbon dioxide, all per volume matrix rock. so, we have:(Berawala & Østebø Andersen, 2019a)

$$A = A_f + A_m + A_c \tag{13}$$

After reaction between methane and carbon dioxide and equilibrium between two component, the area per volume rock A_i occupied by methane and carbon dioxide is as below:

$$A_c = A \, \frac{K_m P_c^{n_c}}{K_c P_m^{n_m} + K_c K_m + K_m P_c^{n_c}} \quad , A_m = A \, \frac{K_c P_m^{n_m}}{K_c P_m^{n_m} + K_c K_m + K_m P_c^{n_c}} \tag{14}$$

for the function of these parameters in mole balance computation we have:

$$a_i \left[\frac{mole}{vol\ dry\ rock}\right] = A_i \left[\frac{area}{vol\ dry\ rock}\right] S_{m,i} \left[\frac{mole\ monolayer}{area\ monolayer}\right] n_i \left[\frac{mole\ multilayer}{mole\ monolayer}\right] \tag{15}$$

In the similar way, possible to calculate the adsorbed mass per volume W_i as below:

$$W_i \left[\frac{mass}{vol\ dry\ rock}\right] = a_i \left[\frac{mole}{vol\ dry\ rock}\right] M_{w,i} \left[\frac{mass}{mole}\right] \tag{16}$$

For conserved property we have:

$$\phi \rho_g x_i + (1 - \phi) a_i \tag{17}$$

If $\rho_g(P_t) = \rho_{g,sc} b_g' P_t$ then we have:

$$\phi \, \rho_{g,sc} b_g' P_t \, \frac{P_i}{P_t} + (1 - \phi) a_i = \rho_{g,sc} b_g' \left(\phi P_i + \frac{(1-\phi) a_i}{\rho_{g,sc} b_g'}\right) \tag{18}$$

On the base of Berawala et al.2019 the term $\frac{(1-\phi) a_i}{\phi \, \rho_{g,sc} b_g'}$ was adsorbed component in Pa, but in this work due to the compaction effect in matrix and variable porosity, we need to make adsorption component independent of porosity variation, so in new definition the term $\frac{a_i}{\rho_{g,sc} b_g'}$ is equal to adsorbed component.

$$\hat{a}_i = \frac{a_i(P_m, P_c)}{\rho_{g,sc} b_g'} \tag{19}$$

2.9. Effective Radius Calculation Due to Adsorption/Desorption

We knew from before that due to the presence of gas the outer layer of pore walls will be covered by gas bubbles, therefore occupied part of space in nanopores. The effective radius for free real gas is: (Xiong et al., 2012)

$$r_{eff} = r - d_m \, \theta \tag{20}$$

$$\theta = \frac{P/Z}{P_L + P/Z} \tag{21}$$

θ if we consider ideal gas ($Z = 1$) we gain:

$$\theta = \frac{P}{P_L + P} \tag{22}$$

θ is ratio of adsorbed specific surface area by component, (m2 / m3 rock) on specific surface area, (m2 / m3 rock) so we have:

$$\theta = \frac{A_i}{A} \quad (i = m, c) \tag{23}$$

A_i is adsorbed specific surface area by component and A is specific surface area. So, we have:

$$r_{eff} = r - d_m \frac{K_i P_i^{n_i}}{K_c P_m^{n_m} + K_c K_m + K_m P_c^{n_c}} \quad (i = m, c) \tag{24}$$

d_m is the methane diameter, between CO_2 and CH_4, the diameter of methane is bigger than carbon dioxide, so the molecule with a bigger diameter defines the outer layer of pore wall coverage. r is a mean pore radius that is our given data from Marcellus shale and is 100 nanometer. With effective radius correction possible to implement in the main formula for better estimation of gas production. Table 2-2 is described the advantages and disadvantages of different adsorption isotherms.

Isotherm	Advantages	Disadvantages
Langmuir	Best one parameter isotherm	Ignore adsorbate/adsorbate interactions
Freundlich , Toth	Two parameters	No physical basis for equation
Multistic	Many parameters	Good for inhomogeneous surface. Wrong physics for single crystals.
Tempkin Flower Slygin-Frumkin	Account for adsorbate/adsorbate interactions in an average sense	Dose not consider how the adsorbate layer is arranged
Lattice gas	1-Complete description of adsorbate/adsorbate interactions for commensurate layers 2- Predicts arrangement of adsorbed layer	1-Require a computer to calculate isotherm 2-Assume commensurate adsorption 3-Parameters used in the model are difficult to determine.

Table 2-2 Comparison of the advantages and disadvantages of several adsorption isotherms.

(MASEL, 1996)

2.10. Geomechanical Compaction

The general structure of this section is an impression from a previous master thesis (Nergård, 2018). In shale gas reservoir modeling it is important to consider permeability alteration due to overburden pressure. It is typical in conventional reservoirs to consider the permeability insensitive to compaction due to the large pore throats of the rock and rocks may not be under complete closure when the effective stress increasing (Faulkner & Rutter, 1998). On the base of former researches, increasing or decreasing of the permeability is dependent on pressure, when there is production due to pressure depletion, therefore, increasing of effective stress or overburden pressure cause decrease in permeability (Bustin, Bustin, & Cui, 2008; Soeder, 1988; F. P. Wang & Reed, 2009).

2.10.1. Effects of geomechanical compaction on shale gas reservoirs

Wu et al. (2014) proposed a simple model approach, easy to integrate geomechanics with the two-phase flow in unconventional reservoirs. This model demonstrates the effect of stress-dependent matrix gas permeability versus effective stress for a horizontal well with 10-levels of hydraulic fracture-system in uniform and tight porous media and fractured reservoir. As it is shown in Figure 2-4 The effect of effective pressure on gas permeability in different shale gas formations. that during production, there will be pore pressure reduction and so, increase the effective stress and consequently decrease the gas permeability. (Y.-S. Wu et al., 2014).
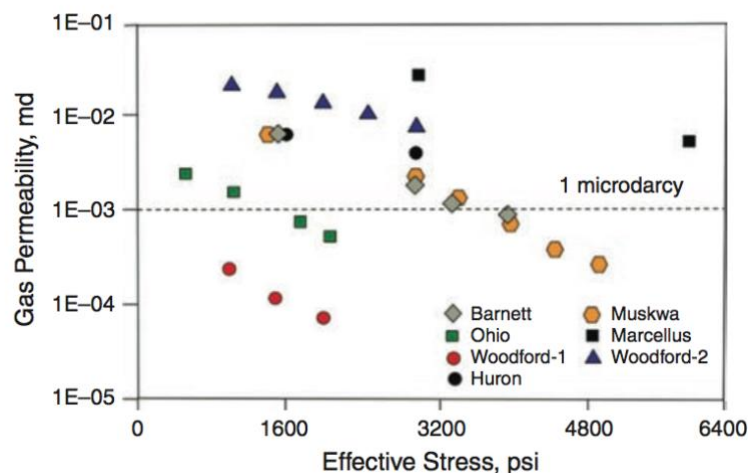
Figure 2-4 The effect of effective pressure on gas permeability in different shale gas formations.

In the above figure, it is clear that sensitivity of Muskwa shale gas permeability versus effective stress is more than other types of shale gas formations.

(Y.-S. Wu et al., 2014)

2.10.2. Effect of Geomechanics in Shale Gas Reservoir Modelling
2.10.2.1 Stress Dependent Matrix

There are lots of correlation that have been used to tie between matrix porosity and effective stress. (Davies & Davies, 1999; Rutqvist, Wu, Tsang, & Bodvarsson, 2002; Winterfeld & Wu,

2011). One of the most typical correlation represented by Rutqvist :(Davies & Davies, 1999; Rutqvist et al., 2002).

$$\phi^m(P_g) = \phi_r + (\phi_0 - \phi_r)e^{-\eta_m \sigma'_m} \qquad (25)$$

It is possible to conclude initial matrix porosity by below formula:

$$\phi_i^m = \phi_r + (\phi_0 - \phi_r)e^{-\eta_m \sigma'_{m,i}} \qquad (26)$$

The $\phi(P_g)$ is porosity dependent of gas pressure, ϕ_r is the high effective stress porosity, ϕ_0 is the porosity at zero effective mean stress ($\sigma_m = 0$), ϕ_i^m is the matrix porosity at initial reservoir condition, η_m is the matrix porosity stress dependent factor in Pa^{-1} and σ_m is the mean effective stress in Pa. Raghavan and chin (2004) proposed another approach for integration of stress dependent matrix pores which is mainly related to the vertical overburden load and reservoir pressure (Raghavan & Chin, 2002; J. Wang et al., 2017).

$$\sigma'_m = \bar{\sigma}_{m,tot}(\sigma_{ob,v}) - P_g \qquad (27)$$

Identically, the initial mean effective stress $\sigma'_{m,i}$ can be expressed:

$$\sigma'_{m,i} = \bar{\sigma}_{m,tot}(\sigma_{ob,v}) - P_{init} \qquad (28)$$

Where $\bar{\sigma}_{m,tot}$ is the total mean stress pressure which is a function of $\sigma_{ob,v}$ (overburden load) and is relatively an invariable value for the system studied. It also assumes that the effective porosity and permeability of the rock just tie in with the mean effective stress. Substituting (33) and (34) into (35) and (36) for σ'_m and $\sigma'_{m,i}$, respectively, so the equations will be:

$$\phi(P_g) = \phi_r + (\phi_i^m - \phi_r)e^{-\eta_m(P_{init}-P_g)} \qquad (29)$$

The impact of effective stress on gas permeability in shale gas investigated by Soeder (1988), Bustin et al. (2008), and Wang and Reed (2009). The stress-dependent relationship between permeability and effective stress derived by Raghavan and Chin (2004) is more compatible with experimental data:(Bustin et al., 2008; Raghavan & Chin, 2004; Soeder, 1988; F. P. Wang & Reed, 2009).

$$K^m(P_g) = K_0^m e^{-\Psi_m \sigma'_m} \qquad (30)$$

Where K_0^m is the matrix permeability when the effective mean stress is zero ($\sigma'_m = 0$) and Ψ_m is the permeability stress-dependent factor for a matrix with the unit of Pa^{-1}. The initial permeability for the matrix is as below:

$$K_i^m = K_0^m e^{-\Psi_m \sigma'_{m,i}} \qquad (31)$$

By substituting (35) and (36) into (38) and (39) respectively, the absolute permeability of matrix depend on reservoir pressure and we obtain:(J. Wang et al., 2017).

$$K^m(P_g) = K_i^m e^{-\Psi_m(P_{init}-P_g)} \qquad (32)$$

A substitute approach of integrating the stress-dependent matrix pores is the usage of a table-lookup approach for correlation of reservoir porosity and permeability as a function of effective mean stress by laboratory studies for a given shale (Yu & Sepehrnoori, 2014).
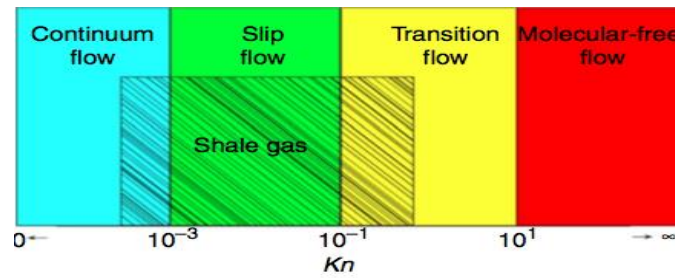
Figure 2-5 Gas-transport regimes in nanopores.

(J. Wang et al., 2017)

2.11. Fractal Dimensions in Shale Gas Reservoirs

With high-resolution images, it is possible to find detailed information about pore with size ranges of nanometers to micrometers. But the relation of this information to transport properties of a sample as the same size as a core is challenging. The observed self-similarity of the pores proved that the pore space of shale could be fractal. R.C.K proposed "the fractal dimension analysis of the computer tomography (CT) technique for different shale classification" (Ōtani & Obara, 2004). Researchers used fractals for simulation of transport properties of porous media. There has been lots of research in tight formations for capturing the heterogeneity of stimulated volume, complex geometries of fractures and variation in apparent and relative permeabilities (Sakhaee-Pour & Li, 2016). In recent years researchers found a combined method for better understanding of effective porosity and pore characteristics and relationship between nanoscale properties of porosity to microscale cores. They mixed the porosity method with an improved porosity method considering fractal characteristics (Lin et al., 2018). As we know the core composed of rock skeleton and pore space, in theory, two parts of core CT image should be different in grayscales, but it is not in reality due to constraints of imaging equipment and other parameters. Furthermore, the edge of pores and skeletons is unclear, which causes difficulty in image segmentation. In the porosity method, the core porosity measured by the liquid saturation or gas expansion method. Porosity shows the share of pore space in rock and the quality of image segmentation will improve by a combination of the porosity to the CT image segmentation. But in improved porosity method that combined with fractal rules, divides images based on the calculated porosity of each image instead of the measured porosity of the whole core (Lin et al., 2018).

3. Mathematical Model

This model is on the base of previous work by Berawala and Andersen (2019) and the geomechanical effect model in this work is on the base of a previous thesis written by Edgard with supervisory of Berawala and Anderson (2018). In this model CO_2 injection to hydraulically fractured shale gas reservoirs with geomechanical compaction effect in the matrix, effective radius in the matrix, adsorption/desorption in the matrix and kerogen, diffusivity, gas concentration, and apparent permeability will be considered.

3.1. Fracture/Matrix-Modelling Assumptions

We need a simple model that represents the main aspects of shale gas production. The main presumptions for matrix and fracture are as below:

1. Rock properties (porosity, permeability) for fracture and matrix are heterogeneous.
2. Primarily shale matrix consists of methane component (CH_4) only, in the form of free gas and adsorbed phase.
3. The carbon dioxide that we inject in gaseous form it can be seen in both gaseous and adsorbed form in the matrix.
4. The composition and flow properties of free and adsorbed gas components assumed to be the same.
5. Single-phase flow of gas is considered (we consider that just dry gas and infinitesimal amount of oil and water).
6. An individual fracture drains gas from the surrounding matrix.
7. Gas is produced from the fracture to the well at constant well pressure.
8. The fracture width assumes constant.
9. Gas desorption is pressure dependent, which is studied by Langmuir multicomponent isotherm.
10. We consider the gas as an ideal gas and has constant viscosity.
11. We consider geomechanical compaction within the matrix and consider fracture constant.
12. We consider these mechanisms in the matrix: adsorption, desorption, compaction effect on porosity and permeability, effective radius, diffusivity, gas concentration, apparent permeability.

3.2. Geometry

We assume a fracture that extends perpendicularly from the well and then considers the situation of y-axis along the fracture pointing away from the well perforation, where $y = 0$. The fracture length is L_y and the constant width is $2b$. The gas is restored from the matrix to fracture in the way that is perpendicular to fracture ($x - direction$). We assume $x = 0$ at the right-hand-side fracture/matrix interface. The fracture and matrix ranges are given by:

$$\Omega^f = \left[(x, y): -2b < x < 0 ; 0 < y < L_y\right] \tag{33}$$

$$\Omega^m = \left[(x, y): -2b - L_x < x < -2b; \ 0 < x < L_x ; 0 < y < L_y\right]$$

We assume that the fracture systems will be repeated (equally spaced fractures), so we have a natural no-flow boundary at $x = L_x$ [the matrix half-length (symmetry)]. We solve equations just for one side of the system, but we account for both sides for production (Berawala et al., 2019). For more simplification of our model, fracture geometry is considered rectangular shape.
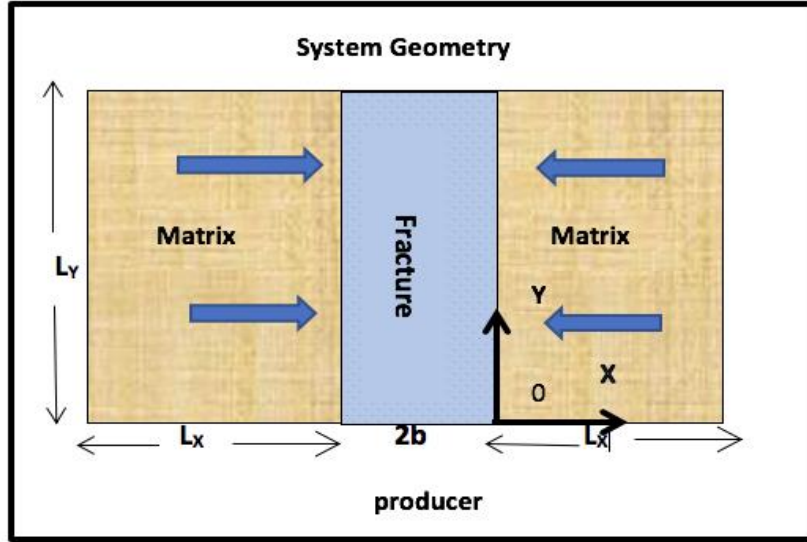
Figure 3-1 Geometry of model for fixed fracture width.

3.3. Modelling Approach
3.3.1. Mass Conservation

The moles of gas changes because of flow in and out of the interface $\partial\Omega$ with area A, for the composition of two gases (CO_2 and CH_4) we have: (Chen, Huan, & Ma, 2006).

$$\partial_t \int_\Omega [\phi\, \rho_g x_i + (1-\phi)\, a_i]dV = -\int_{\partial\Omega}(\rho_g u\, x_i) \cdot n\, dA, \tag{34}$$

where $\rho_g(p_t)$ gas molar density (moles of gas-phase per volume gas mixture), ϕ is porosity, u is the Darcy-mass-flux vector, n is the unit-normal vector pointing out of Ω, x_i mole fraction of component ($i = c, m$), a_i is amount adsorbed component i (in moles component per volume matrix rock), and p_t is total gas pressure. The flux vector u is here and dependent to pressure by Darcy's law:

$$u = -\frac{k^m}{\mu_g}\nabla p_t, \qquad\qquad p_t = p_m + p_c \tag{35}$$

k^m is the permeability of gas in the matrix and μ_g is the gas viscosity, which is set constant. The partial pressure P_i associated with N_i moles of component residing in the gas mixture volume V_g (which is possible to share with other components is defined by the real law) (Chen et al., 2006).

$$P_i V_g = z N_i RT \tag{36}$$

$$(P_1 + P_2 + \cdots + P_n) = z(N_1 + N_1 + \cdots + N_n)RT$$

$$P_t V_g = z N_t RT$$

The latter formula is derived from the first and concerns the total pressure from the gas mixture. z stands for the deviation factor from an ideal gas, R is the gas constant and T is the absolute temperature.

3.3.1.1 Density-pressure relations

Molar gas-phase density at reservoir and surface conditions (sc) follow directly as:

$$\rho_g = \frac{N_g}{V_g} = \frac{P_t}{zRT}, \qquad \rho_{g,sc} = \frac{N_g}{V_{g,sc}} = \frac{P_{sc}}{RT_{sc}} \tag{37}$$

z presumed constant at reservoir conditions and unity at standard condition, so we could find the inverse gas volume factor b_g as the ratio of the volume taken by a gas mixture at standard conditions to the volume it takes at reservoir conditions:

$$b_g(P_t) = \frac{\rho_g}{\rho_{g,sc}} = P_t \frac{T_{sc}}{P_{t,sc}\, zT}, \quad b_g'(P_t) = \frac{T_{sc}}{P_{t,sc}\, zT} \;, \quad \rho_g(P_t) = \rho_{g,sc}\, b_g'\, P_t \tag{38}$$

In the above formula the derivative of b_g with respect to p_t that is a constant (with a unit of inverse pressure) to write a combined relationship between gas density and total pressure. Mole fractions x_i and molar follow from the gas law:

$$x_i = \frac{N_i}{N_t} = \frac{P_i}{P_t} \; (i = m, c) \tag{39}$$

C_i is the concentration of gas component i (in mole per volume gas mixture) and molar concentrations of gas component C_i follow from the gas law directly :

$$C_i = \frac{N_i}{N_t} = \frac{P_i}{zRT} \; (i = m, c) \tag{40}$$

$D_{i,e}$ is the effective molecular diffusion coefficient of gas components depends on the free molecular diffusion coefficient $D_{i,f}$ and the tortuosity τ of the porous medium as below: (He, Lv, & Dickerson, 2014).

$$D_{i,e} = \frac{D_{i,f}}{\tau} \qquad (i = m, c) \tag{41}$$

3.3.1.2 Shale-Gas Adsorption

The a_i is an adsorbed component parameter that is pressure-dependent and described as below: (Berawala & Østebø Andersen, 2019b). The conserved property $\phi \rho_g x_i + (1 - \phi)\, a_i$ can be defined as below:

if $\rho_g(P_t) = \rho_{g,sc}\, b_g'\, P_t$ and $\hat{a}_i = \frac{a_i(P_m, P_c)}{\rho_{g,sc} b_g'}$

So, for conserved property we have:

$$\phi\, \rho_{g,sc} b_g' P_t \frac{P_i}{P_t} + (1 - \phi)\, a_i = \phi\, \rho_{g,sc} b_g' P_i + (1 - \phi)\, \hat{a}_i\, \rho_{g,sc} b_g' = \rho_{g,sc} b_g' (\phi\, P_i + (1 - \phi)\hat{a}_i)$$

3.3.1.3 Fracture Domain

If In the fracture, we ignore gas adsorption (i.e., $a_i^f = 0$). The fracture width defined by $2b$, regarding volume $dV = 2b\, h\, dy \to 0$, we have:

$$\partial_t(\phi\,\rho_g\,x_i 2b) = \partial_y(\rho_g u\,x_i\,2b) + (\rho_g u\,x_i)_{x=-2b,y} - (\rho_g u\,x_i)_{x=0,y} \qquad (42)$$

Because the fracture is surrounded symmetrically by the matrix, the two source terms are calculated identically,

$$(\rho_g u\,x_i)_{x=-2b,y} = -(\rho_g u\,x_i)_{x=0,y} \qquad (43)$$

So for constant fracture width with the rectangular shape we have:

$$\partial_t(\phi\,\rho_g\,x_i b) = -\partial_y(\rho_g u\,x_i\,b) - (\rho_g u\,x_i)_{x=0,y} \qquad (44)$$

If we substitute the parameters in above formula:

$$\partial_t(\phi\,P_t\,\rho_{g,sc}b_g'\,b\,\frac{P_i}{P_t}) = -\partial_y(-\frac{k^f}{\mu_g}\partial_y(p_t)P_t\,\rho_{g,sc}b_g'b\,\frac{P_i}{P_t}) - (-\frac{k^m}{\mu_g}\partial_x p_t\,P_t\,\rho_{g,sc}b_g'\,\frac{P_i}{P_t})_{x=0,y} \qquad (45)$$

After some simplifications in above formula, in final form we have :

$$b\,\phi\,\partial_t(p_i) = \frac{k^f}{\mu_g}\,b\,\partial_y(p_i\,\partial_y(p_t)) + \frac{k^m}{\mu_g}(p_i\,\partial_x(p_t))_{x=0,y} \quad (i=m,c) \quad (x,y \in \Omega^f) \qquad (46)$$

3.3.1.4 Matrix Domain

In the matrix, just we have the flow in the x-direction (toward the fracture), whereas flow in the y-direction is negligible. Considering a volume $dV = dx\,dy\,h \to 0$, as a general formula of compressible gas flow which includes advection, diffusion, and adsorption is given by (modified from Chen et al.):(Chen et al., 2006)

$$\partial_t[\phi\,\rho_g x_i + (1-\phi)\,a_i] = -\partial_x(\rho_g u\,x_i) + \partial_x\,(D_{i,e}\,\phi\,\partial_x\,C_i) \qquad (47)$$

As it is clear in above, there are two gas components, so we need to consider both reactions of CO_2 and CH_4 on the rock surface and their pressures for competitive adsorption.

If we put the equations (35), (38), (39), (40) and (41) in (47), so we have:

$$\partial_t[\phi^m P_t\,\rho_{g,sc}b_g'\,\frac{P_i}{P_t} + (1-\phi)\,\hat{a}_i\,\rho_{g,sc}b_g'] = -\partial_x(-\frac{k^m}{\mu_g}\,\partial_x(P_t)\,P_t\,\rho_{g,sc}b_g'\,\frac{P_i}{P_t}) +$$

$$\partial_x(\frac{D_{i,f}}{\tau}\,\phi^m\,\partial_x(\frac{P_i}{zRT}))$$

After some simplification in the above form we have:

$$\partial_t(\phi\,P_i + (1-\phi)\hat{a}_i) = \frac{1}{\mu_g}\partial_x(\,k^m\,\partial_x(P_t)\,P_i) + \widehat{D}_i\,\partial_x(\,\phi^m\,\partial_x(\,P_i))\quad,(i=m,c) \qquad (48)$$

$$(x,y\in\Omega^m)$$

For diffusivity term we have :

$$\widehat{D}_i = \frac{1}{\rho_{g,sc}b_g'}\;\frac{D_{i,f}}{\tau zRT} \qquad (49)$$

3.3.2. Stress Dependent Matrix Porosity

For derivation and description of stress-dependent matrix porosity in this part, it is referred to as equations (25),(26),(27) and (28) in chapter 2. So stress-dependent matrix porosity formula is as follow:

$$\phi\left(P_g\right) = \phi_r + (\phi_i^m - \phi_r)e^{-\eta_m(P_{init}-P_g)} \tag{51}$$

3.3.3. Initial and Boundary Conditions

The equations of flow must be calculated with the initial and boundary conditions.
Initially, at $t = 0$, the matrix contains free CH4 gas with initial pressure P_{m0} :
$$P_m(t = 0) = P_{m0} = P_{init}, \qquad P_c(t = 0) = P_{c0} = 0 \tag{50}$$
The adsorbed gas is in equilibrium with this composition:
$$a_m(t = 0) = a_m(P_{m0}, P_{c0}), \quad a_c(t = 0) = 0. \tag{51}$$
The fracture and matrix have the same initial pressure P_{init} at $t = 0$.
The perforation is defined at $y = 0$ with a known pressure, (Jiang & Yang, 2018)
$$P_m^f (y = 0) = 0, (x \in \Omega^f) \tag{52}$$
$$P_c^f (y = 0) = P_{well},$$

The open boundary at $x = 0$ acts with defined partial pressures as a function of time. And around fracture wall in x direction we have: (Berawala et al., 2019)
$$P_i|_{x=0^-} = P_i|_{x=0^+}, \tag{53}$$

The fracture is closed (or has negligible production) from the matrix in the y-direction. Similarly, the matrix because of symmetry, has no flow at its outer boundary.
$$\partial_y P_i|_{y=L_y} = 0, \partial_x P_i|_{x=L_x} = 0, \tag{54}$$

3.3.4. Summary of Model

The system for gas flow in fracture matrix is :
$$b\, \phi^f\, \partial_t(p_i) = \frac{k^f}{\mu_g}\, b\, \partial_y(p_i \partial_y(p_t)) + \frac{k^m}{\mu_g}\, (p_i\, \partial_x(p_t))_{x=0,y} \quad (i = m, c)\ (x, y \in \Omega^f) \tag{55}$$

$$\partial_t(\phi\, P_i + (1 - \phi)\, \hat{a}_i) = \frac{1}{\mu_g} \partial_x(k^m\, \partial_x(P_t)\, P_i) + \hat{D}_i\, \partial_x(\phi\, \partial_x(P_i)) \quad (i = m, c), \tag{56}$$
$$(x, y \in \Omega^m)$$

$$\hat{D}_i = \frac{1}{\rho_{g,sc}b_g'}\, \frac{D_{i,f}}{\tau z RT} \tag{57}$$

$$B_i = \frac{S_{m,i}\, n_i}{\rho_{g,sc}b_g'} \tag{58}$$

$$\hat{a}_i = \frac{a_i(P_m, P_c)}{\rho_{g,sc}b_g'} = \frac{S_{m,i}\, n_i A_i(P_m, P_c)}{\rho_{g,sc}b_g'} = B_i A_i(P_m, P_c) \tag{59}$$

Equations (55) and (56) will be solved with consideration of initial and boundary conditions.

4. Simulation Results and Discussion

In this part, we show the performance of model Eqs. (55) and Eqs. (56) by studying its sensitivity to various input parameters. Specially we will consider the recovery factor versus time during methane production and CO_2 injection, reservoir pressure, and gas-recovery curve are affected by matrix and other gas parameters. Gas recovery factor will be reported as a fraction of the mass initially in the reservoir. For the mathematical calculation of the recovery, the Appendix A will be referred. The system will be solved by operator-splitting method that is described by (Agista, Andersen, & Yu, 2019; Andersen, Evje, & Kleppe, 2014; Berawala et al., 2019). This system means that we alternate solving between flow in y direction (fracture diffusion) the flow in x direction (fracture/matrix diffusion and desorption). The numerical-solution approach is defined in Appendix C. The $y - axis$ is discretized into 8 equal cells, whereas the $x - axis$ is divided into 8 equal cells that include also fracture cell.

4.1. Model Input

The parameters that used for inputs of model in Table 4-1 are for the base case that demonstrate gas, rock and transportation properties.

Parameters	Value	Units
Fracture half-width, b	0.02	m
Well bottom-hole pressure, P_{well}	17.24	bar
Fracture length, L_y	10	m
Matrix half-length, L_x	20	m
Fracture permeability, K^f	10	md
Fracture height, h	1	m
Matrix permeability, K^m	10	μd
Gas density at standard conditions, ρ_{sc}	0.7	Kg/std m3
CH_4 well pressure, $P_{m,well}^{inj}$	0	bar
CO_2 well injection pressure, $P_{c,well}^{inj}$	550	bar
Well production pressure $P_{t,well}^{prod}$	150	bar
Initial CH_4 matrix pressure, P_{m0}	350	bar
Initial CO_2 matrix pressure, P_{c0}	0	bar
Real gas deviation factor (ideal gas), Z	1	−
Gas constant, R	8.314	J/mol
CH_4 viscosity, μ_m	0.0184	cP
CO_2 viscosity, μ_c	0.0184	cP
Matrix length, L	0.07	m
Matrix porosity, ϕ^*	0.1	−
Mean pore radius, r_e	100	nm
Reservoir temperature, T^*	323.15	K
Tortuosity of rock, τ	1.51	-
Molar weight of CH_4	$16.04x10^{-3}$	kg/mol
Molar weight of CO_2	$44.01x10^{-3}$	kg/mol
CH_4 Diffusion coefficient, D_m	$1x10^{-8}$	m^2/s
CO_2 Diffusion coefficient, D_c	$1x10^{-8}$	m^2/s
* (Yu, Sepehrnoori, & Patzek, 2016)		

Table 4-1 Input parameters used for reference-case simulations. Reservoir and temperature are representative of Marcellus Shale (Godec, Koperna, Petrusak, & Oudinot, 2013)

The Longmuir-isotherm parameters that taken from (Yu et al., 2016) are representative of Marcellus shale. Otherwise will be stated in the text and other unchanged parameters are held constant, equal to base case. In this work the fracture will be in the reference case and is considered to have a constant width. Adsorption measurements of CH_4 and CO_2 are given from Marcellus, Barnett, and Eagle Ford shale for parametrization of multicomponent adsorption model (Godec et al., 2013; Heller & Zoback, 2014). For a typical specific surface area we have A= $20*10^3$ m2/kg that was performed for our model.

4.2.   Simulation Results

In this part we investigate the deviation of Knudsen number versus pressure and its impact during simulation with core and field scales. In core scale the typical average pore radius is considered 100 nm because the shale samples will be crushed and compacted for better measurements. At field scale, the pore radius is assumed 20 nm. As we had in Eqs. (3) due to inverse relation of Knudsen number with pressure and pore radius the Figure 4-1 will be drawn. As it is clear in the graph below, the Knudsen number is more sensitive to smaller pore radius before 150 bar and the rate of reduction is more in the pore field scale than core scale pore radius. The Knudsen number of 20 nm pore radius is lower than 0.001 in pressure more than 110 bar, So in the field scale for pressures more than 110 bar, the mean free path is lower than pore radius and it means, there is a slip-flow regime in the reservoir. But for the pressures lower than 110 bar in field scale the mean free path is much lower than pore radius, so we have continuum-flow regime in the reservoir. When we investigate the core scale, the Darcy regime or viscous flow is dominant in all ranges of pressure and when there is a viscous flow in porous media, probability of collision between fluid molecules are more than the probability of collision of molecules with pore wall.
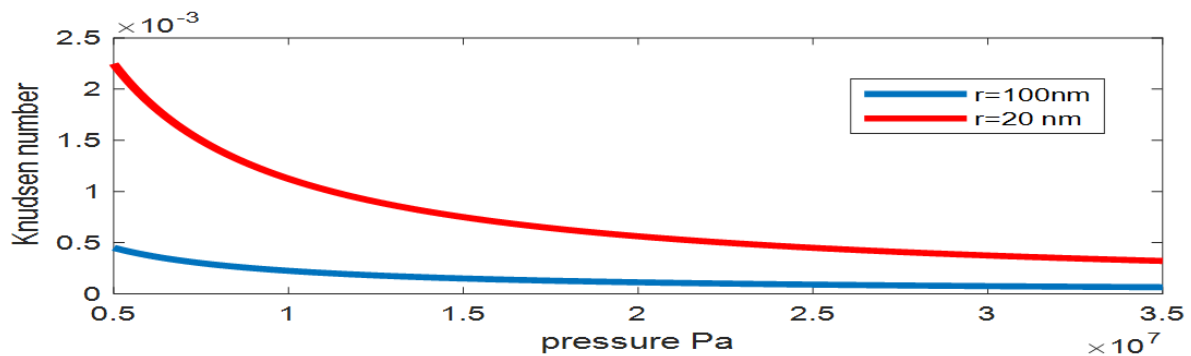
Figure 4-1 Knudsen number versus pressure

4.3.   Base Case with Cyclic CO2 injection

In below Figure 4-2 the base case graph is shown, the model defined in total of 1000 days with 4000 steps, we produce methane for 200 days and then inject carbon dioxide for the next 200 days, so we do the same procedure till the end of 1000th day. In the recovery graph (right) during the first 200 days of CH_4 production the ultimate recovery is around 55 percent and then in the first period of CO_2 injection, recovery is still as the same as last production period,

but for the second period of production the recovery at the end of 200th day increased to 70 percent of methane recovery and In the last period of production the recovery increased to 80 percent. In this model we consider all main mechanisms such as adsorption, diffusion and compressibility of shale reservoir. The pore radius is on the base of field scale (20nm). In the left side of the below graph the blue line is free mass of gas in the fracture, as you can see due to narrow width of fracture (0.02 m) during CH_4 production the amount of free mass is negligible. In yellow line during the first 200 days, because of pressure depletion the adsorbed methane desorbs and converts to free methane molecules and produce through the matrix and then fracture in the well. In second 200 days we have CO_2 injection and when we compare yellow line with orange line shows that free mass of methane in the matrix convert to adsorbed mass and attach to the surface of kerogen due to pressure escalation and the GCIP is constant. In the third 200 days of production the adsorbed mass of gas desorbed and convert to free gas. In the second period of CO_2 injection, lower amount of free methane covert to adsorbed methane, due to more preference of carbon dioxide substitution with methane on the surface of kerogen, lower amount of methane remained.
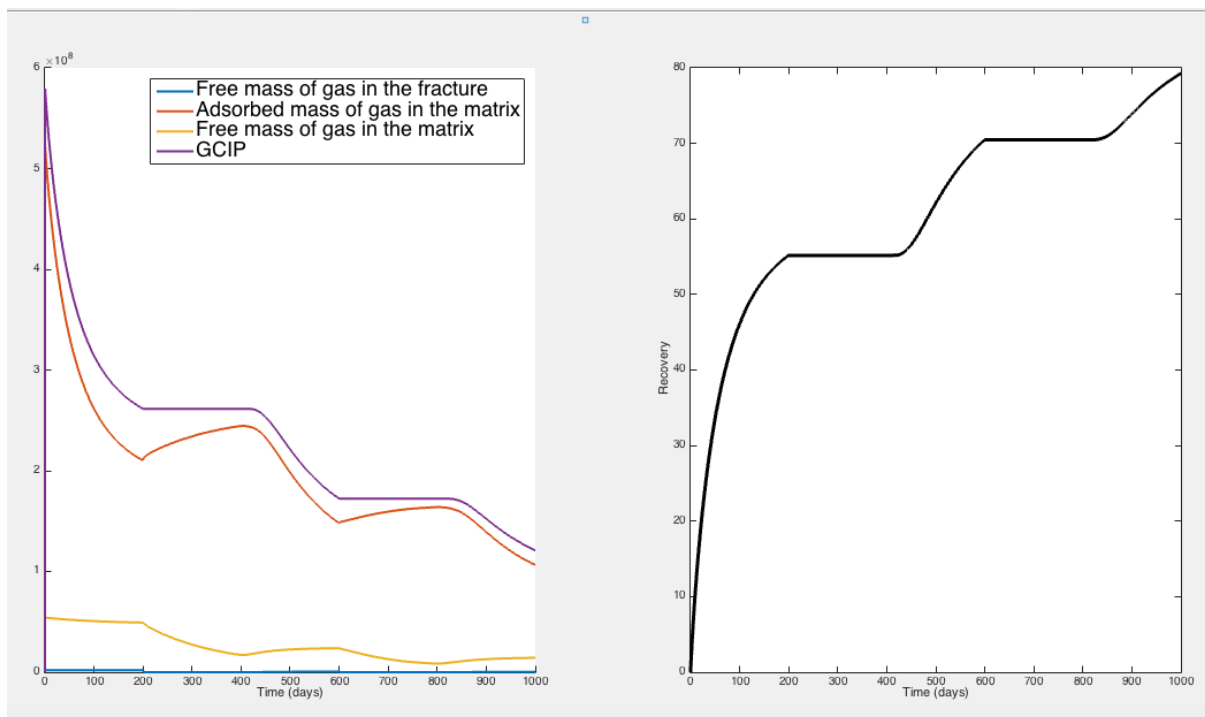
Figure 4-2 (left) free mass of gas in the fracture, adsorbed mass of gas in the matrix, free mass of gas in the matrix, GCIP versus time (days) , (right) methane recovery versus time(days)

In the Figure 4-3 (left) the difference of free mass of gas in the fracture with initial condition of free mass of gas in the fracture drawn versus time and it is negative amounts. During the first period of production the free mass of gas in fracture did not change from initial condition so we have a flat line in this period. In first period of CO_2 injection, there is not any methane in the fracture, so the difference is the highest negative. But in the next period of production the amount of methane is lower than the first period of production, so the amount of negative difference is not as much as the first period. In Figure 4-3 (right) in the first period of production the adsorbed mass of matrix will be decreased so the difference going to be high negative from

the initial point, but in first CO_2 injection, due to substitution of methane with CO_2, more methane desorbs and converts to free gas in the matrix.

Figure 4-3 (left) mass difference of free gas in the fracture(mole) versus time(days), (right) mass difference of gas in the matrix(mole) versus time(day)

In the Figure 4-4 (left) during the first period of methane production, due to pressure depletion, adsorbed methane desorbs and converts to free gas in the matrix, but in the first CO_2 injection period, due to high preference of CO_2 adsorption on the surface of kerogen than methane, more methane desorbs and makes more free gas in the matrix and lower adsorbed mass of methane, so the high reduction in the adsorbed mass is clear. In the (right) the difference of GCIP and OGIP is shown, for example the second period of methane production, we produce around 425000 moles methane.
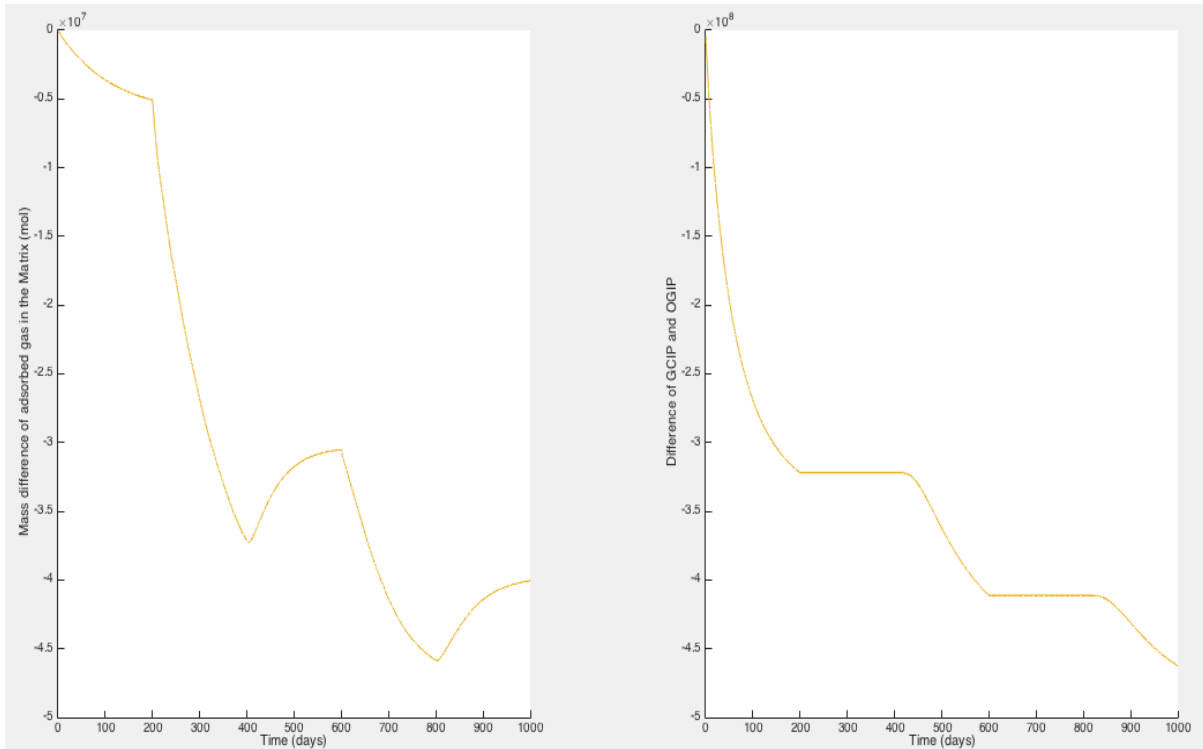
Figure 4-4 (left)mass difference of adsorbed gas in the matrix(mole) versus time(days) , (right) difference of GCIP and OGIP versus time (days)

In the Figure 4-5 (left) the amount of free mass of gas in the fracture during production is around $2.2*10^6$ mole and after start of CO_2 injection it will be zero. In the second period of production, we have carbon dioxide in the system, so the amount of methane will be lower than first production period. In the (right) at first period of production due to pressure depletion the adsorbed methane convert to free methane and then produced, but the rate of free methane production in the matrix is higher than the rate of conversion of adsorbed methane to free methane, so the amount of free CH_4 decreases during production.
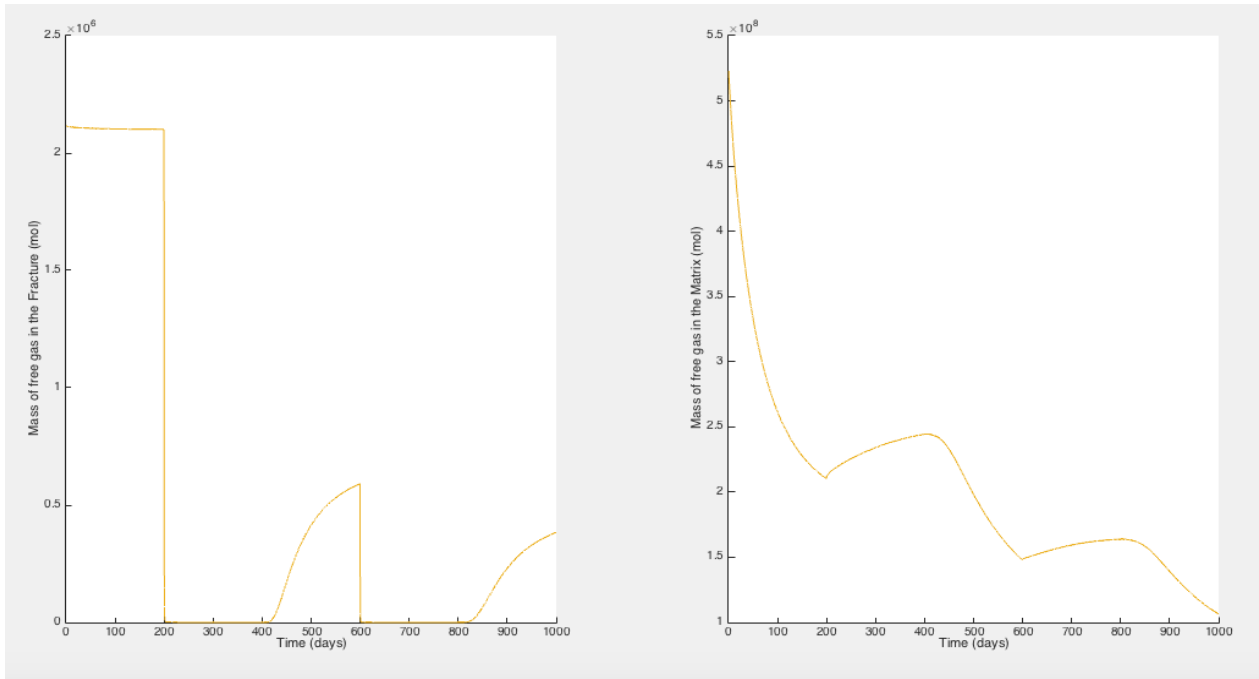
Figure 4-5 (left) mass of free gas in the fracture(mole) versus time(days) , (right) mass of free gas in the matrix (mole) versus time (days)

4.4. Base Case without CO_2 injection

If there is not any carbon dioxide injection into the reservoir, as it is shown in Figure 4-6 (left) the free mass of gas in the fracture will be decrease until being stable around day 500th . In the (right) after pressure depletion, the adsorbed mass, desorb and convert to free mass of gas and go through the fracture. Until the day 500th there will a constant rate of free gas in the matrix due to pressure depletion and stability. It means that reservoir pressure is going to be close to the well pressure.
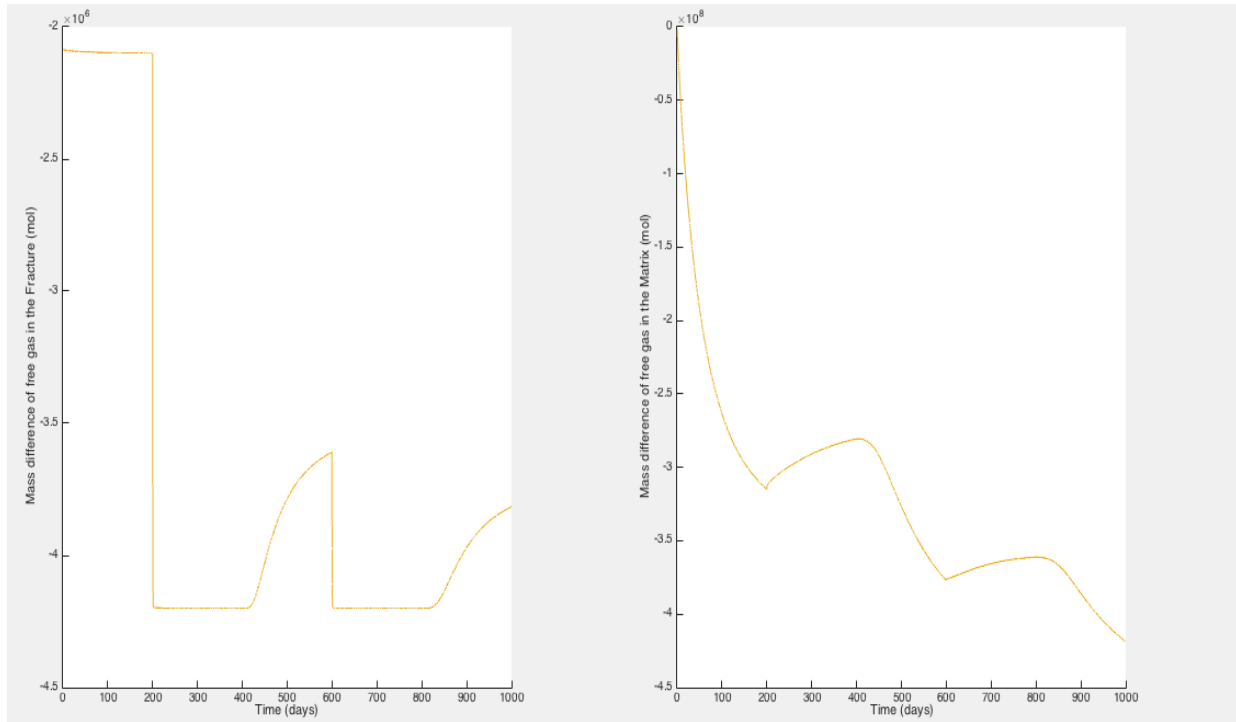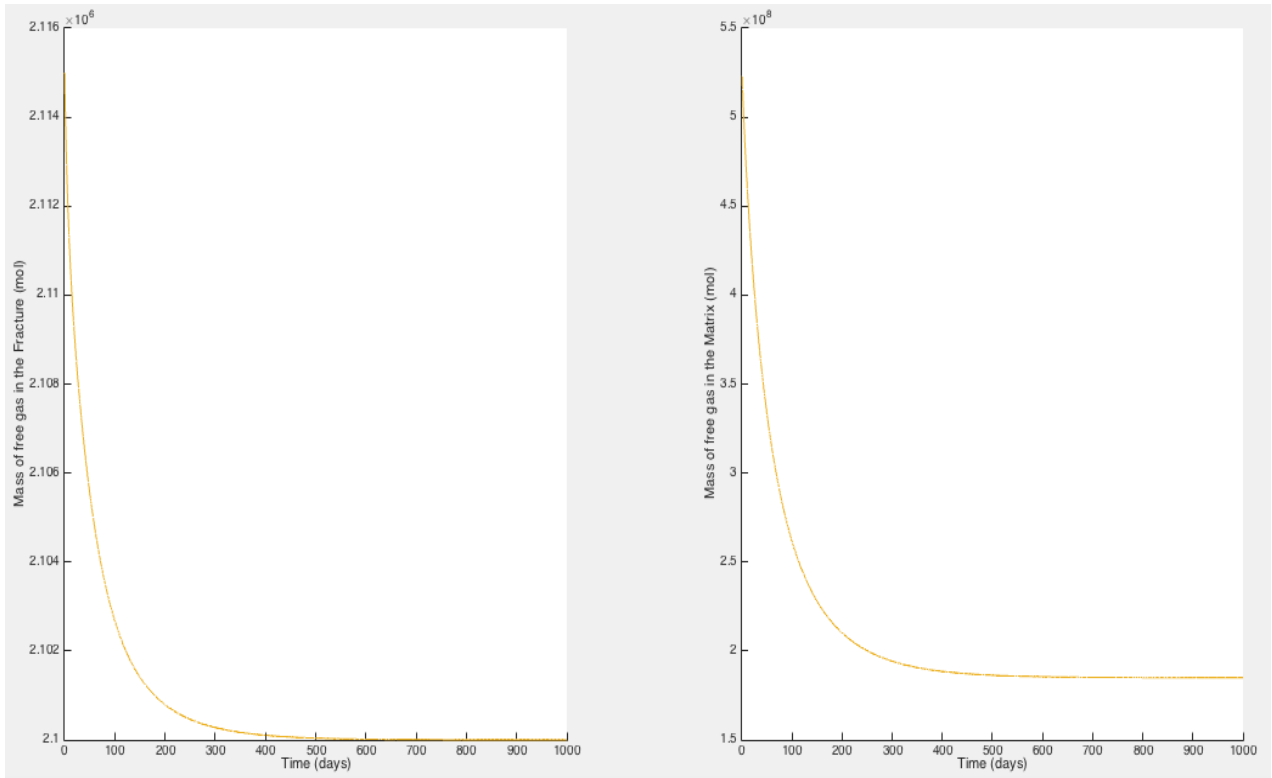
Figure 4-6 (left) mass of free gas in the fracture(mole) versus time(days) , (right) mass of free gas in the matrix (mole) versus time(days)

In the Figure 4-7 (left) the adsorbed mass of gas in the matrix and GCIP will be decreased during production, but after 500 days of production these parameters will be stabilized. As it is clear the free mass of gas in the matrix does not change, it means that the rate of conversion of adsorbed gas to free gas is as the same as free gas production. In the (right) the highest amount of recovery is 60 percent and when the pressure pf reservoir reaches to well pressure, the recovery will be stable. To showing that how much carbon dioxide could increase the recovery, we look at the Figure 4-2 . It is obvious that before first CO_2 injection, the recovery was around 56 percent, but after the first injection, the 15 percent jump in recovery till 71 is seen and for the second injection around 8 percent jump is obvious.
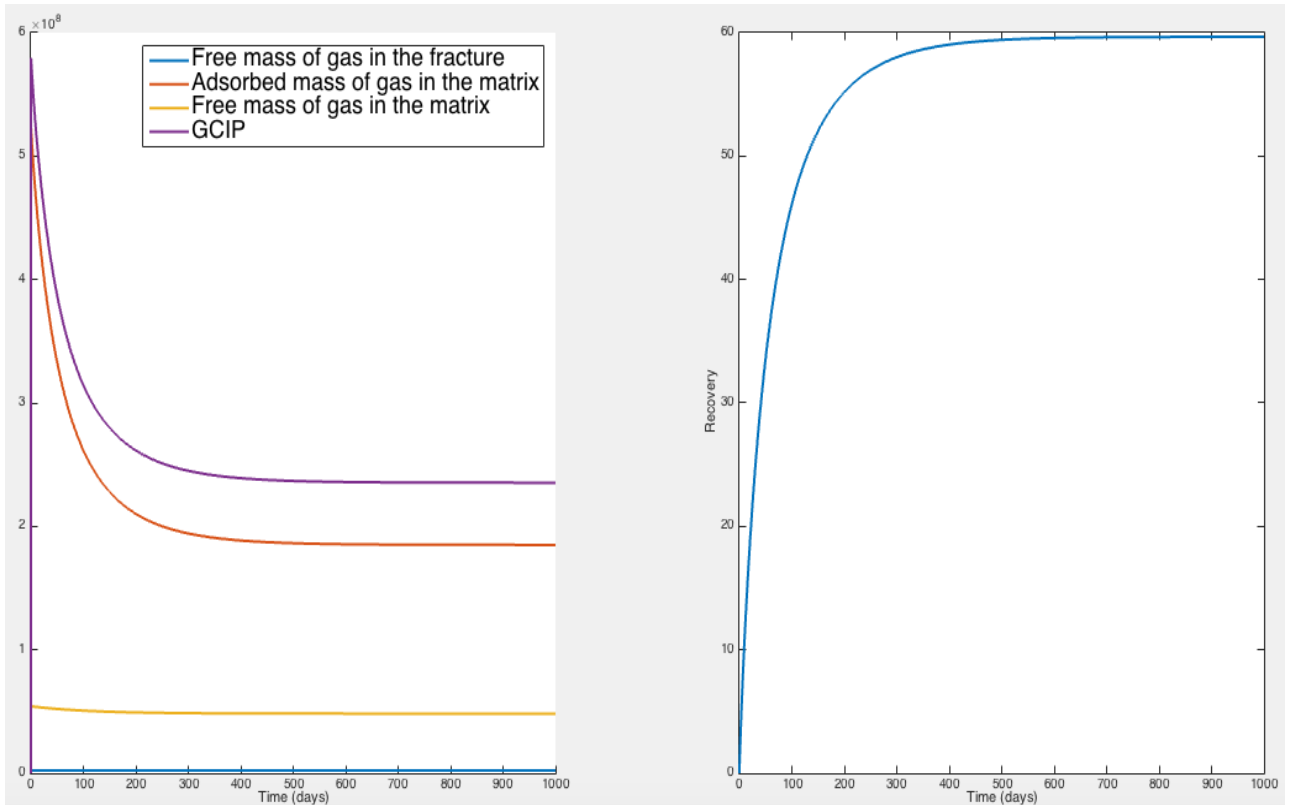
Figure 4-7 (left) free mass of gas in the fracture, adsorbed mass of gas in the matrix, free mass of gas in the matrix, GCIP, (right) recovery of gas versus time (days)

In the Figure 4-8 comparison between three different pore radiuses impact on the of reservoir recovery in combination with CO_2 injection, as it is shown the more pore radius, the more recovery we have. When the pore radius is going to be higher on the base of Eqa. (3) the Knudsen number decreases, and it means mean free path will be much lower than pore radius, so we are shifting to continuum flow. Regarding Eqa. (5) With increasing of pore radius, the apparent permeability will be higher and so the increasing of recovery is reasonable.
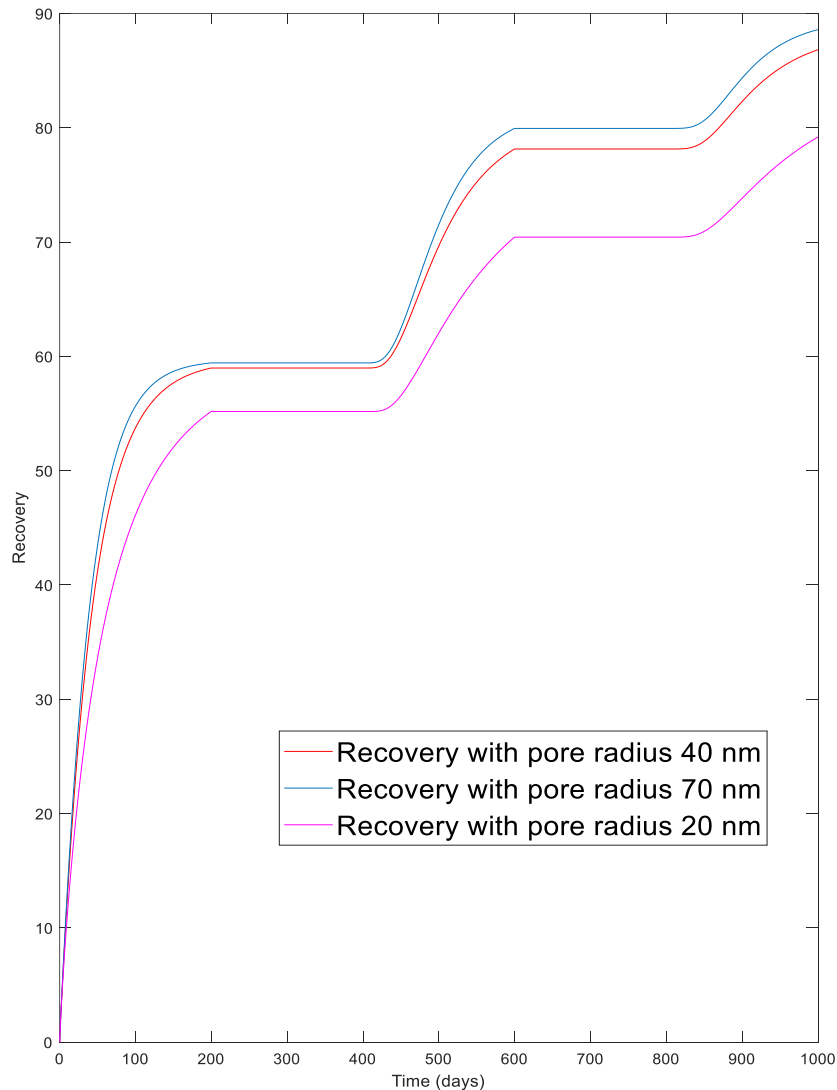
Figure 4-8 recovery versus time(days) with different pore radius, the highest recovery is for pore radius of 70 nm , in the middle is recovery with 40nm of pore radius and the lowest recovery belongs to pore radius of 20 nm

In Figure 4-9 (left) we consider our model with zero adsorption, compressibility and diffusion effect, so there is no change of adsorbed mass of gas in the matrix during production, in the (right) GCIP without adsorption, compressibility and diffusion effect is in yellow line and GCIP with all three mentioned mechanisms is drawn in purple line. When we consider compressibility mechanism in the reservoir, it means during production due to pressure reduction in pore, the pore radius will be smaller than before, firstly we produce because of pressure depletion and secondly compressibility of the rock. In the next step, we consider the effect of adsorption, when gas molecules adsorbed on the surface of kerogen the pore radius decreases. With consideration of all the mechanisms in the first 200 days of production, with regard to desorption, there will be shrinkage of rock grains so the pore radius increase, then

because of pressure depletion and compressibility of rock, the pore radius decrease but as it is clear in the system with all mechanisms included the GCIP is more than the system without them, so the effect of desorption on recovery is more than the pressure depletion.
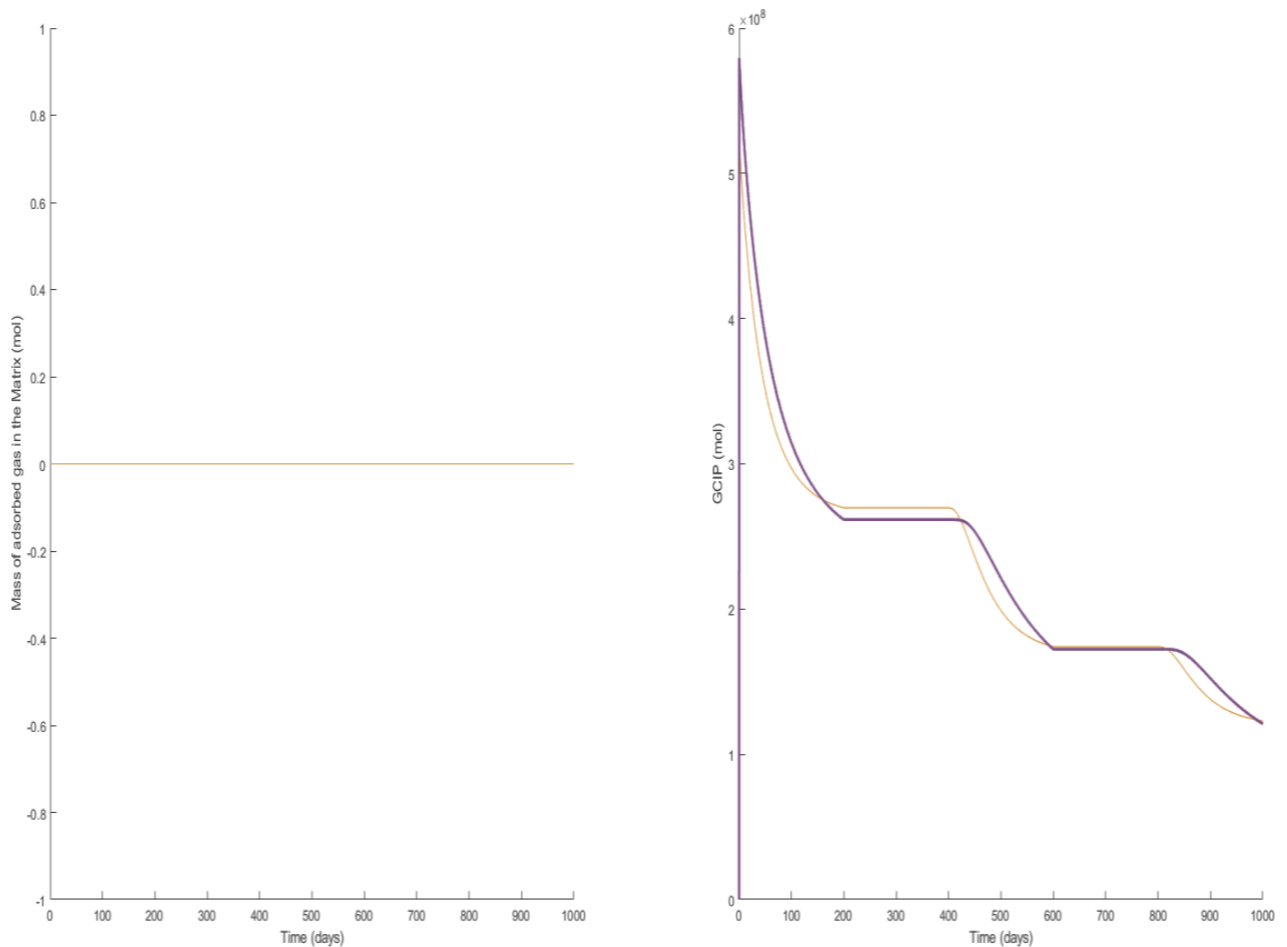
Figure 4-9 (left) mass of adsorbed gas in the matrix(mole) versus time without consideration of adsorption, compressibility and diffusion effect, (right) GCIP versus time (days),the yellow line is without considering of adsorption, compressibility and diffusion effect and purple line is included all mechanisms

In Figure 4-10 we considered different mechanisms effect on the recovery factor. As it is shown in the graph below, the red dot-dash line is the recovery without compressibility and diffusion but this recovery is as the same as recovery without compressibility, it means that the effect of diffusion in our model it is not high enough to improve the recovery. As you can see when included all the mechanisms in compare to system without diffusion, there is not any difference between their recovery, it means the effect of compressibility and adsorption is dominant. But when we compare the recovery of the system without all three mechanisms and the system just without compressibility, it shows that recovery of system with adsorption/desorption effect is lower than the system that does not have this mechanism. As an example during the first 200 days of production, first there will be rock grain shrinkage due to desorption but then the amount of gas bubbles that desorbed, make a barrier in the inner part of pore throat, so the recovery is lower with adsorption/desorption effect.
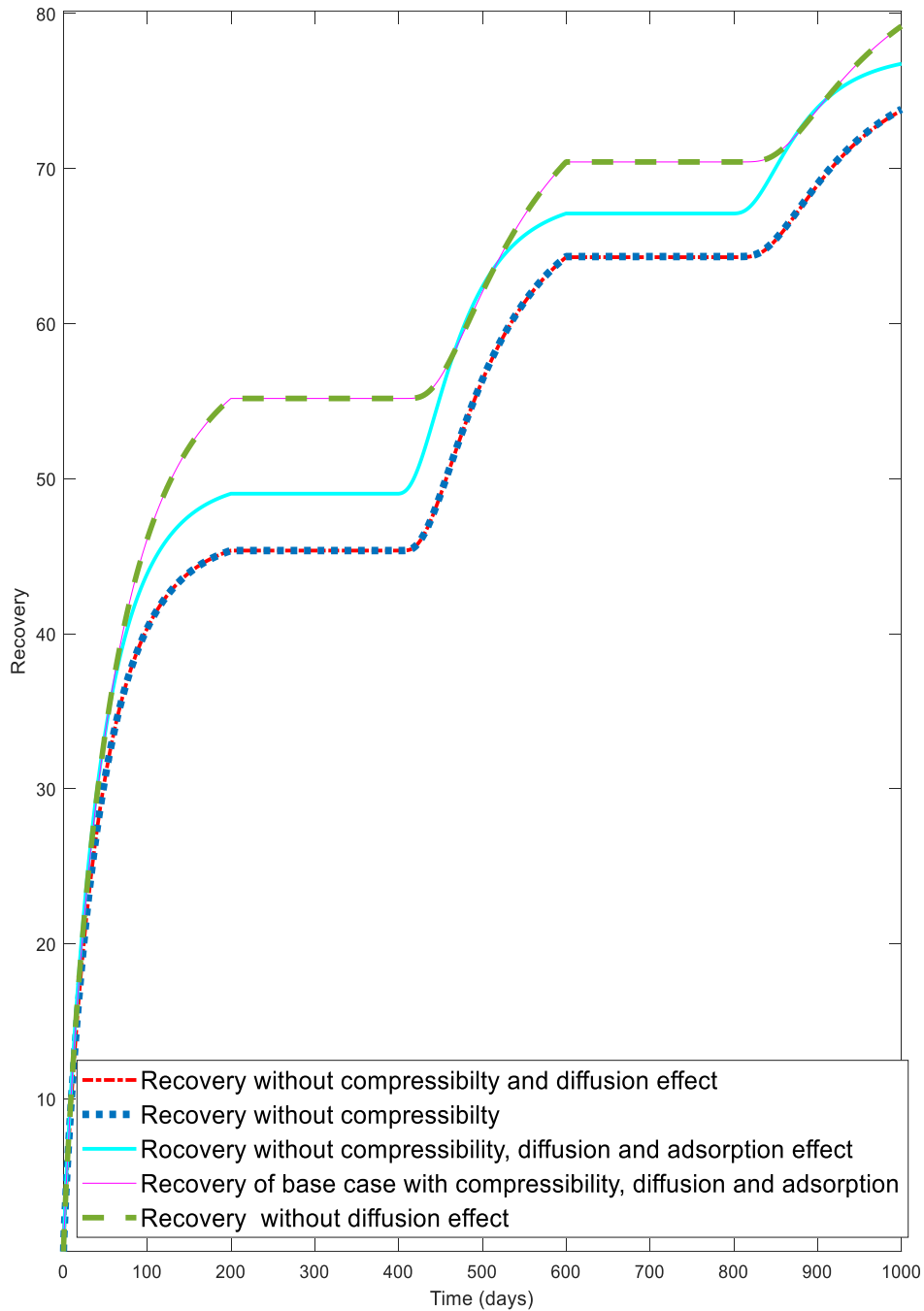
Figure 4-10 recovery of different mechanisms versus time(days)

4.5.   Conclusion

We have investigated combination of multicomponent isotherm for shale-gas EGR by CO_2 injection by assumption of a matrix with a fix induced fracture extending from well perforation under dynamic conditions. In this model we assumed a fixed specific surface area rather than fixed number of sites for surface capacity storage. Gas stored in the matrix as adsorbed and free form, also as a free form in the fracture. Different components have different capacity of adsorption and different surfaces have also different free spaces, so it is important to understand how many moles of specific component adsorbed by kerogen at full capacity and how much

the capacity of surface is covered by different species. In dynamic condition the cyclic CO_2 injection and gas production combined with or without different types of mechanisms such as compressibility, adsorption and diffusivity and here the effect of CO_2 and CH_4 storage, gas recovery, and EGR potential were investigated.

1-Important parameters determine recovery during pressure depletion are reservoir pressure, well pressure and gas in place.

2-If the effective substitution of CO_2 happened with CH_4 in place, So Better EGR is possible and the mixture of these components dilute CH_4 and replace it with higher amounts of carbon dioxide in each period. Not only with increasing of the pressure the more gas comes out of well but also without adsorption, CO_2 has EGR effect.

3-One of the main mechanisms is adsorption, because adsorption improves more the CO_2-EGR potential due to more desorption of CH_4 that release at the same total pressure. Due to pressure reduction during adsorption mechanism, the CO_2 injection goes faster through the matrix.

4- The diffusion is also a key parameter for higher efficiency of EGR method. That is dependent on spatial dimension of matrix, time of diffusion and complex geometry of rock. In our case due to strongly limited effect of diffusion, there was a little benefit of pressure depletion.

5- The compressibility is another fundamental parameters in EGR production, in our model the recovery with considering of compressibility factor is higher than without geo-mechanical effect.

Reference list

Agista, M. N., Andersen, P. Ø., & Yu, Z. (2019). Modelling nanofluid injection in porous media. *Journal of Petroleum Science and Engineering*, *176*, 836–849. https://doi.org/10.1016/j.petrol.2019.02.006

Akkutlu, I. Y., & Fathi, E. (2012). Multiscale Gas Transport in Shales With Local Kerogen Heterogeneities. *SPE Journal*, *17*(04), 1,002-1,011. https://doi.org/10.2118/146422-PA

Ali Beskok, G. E. K. (1999). Report: A Model for Flows in Channels, Pipes, and Ducts at Micro and Nano Scales. *Microscale Thermophysical Engineering*, *3*(1), 43–77. https://doi.org/10.1080/108939599199864

Alnoaimi, K. R., & Kovscek, A. R. (2013, September 30). *Experimental and Numerical Analysis of Gas Transport in Shale Including the Role of Sorption*. Presented at the SPE Annual Technical Conference and Exhibition. https://doi.org/10.2118/166375-MS

Andersen, P. Ø., Evje, S., & Kleppe, H. (2014). A Model for Spontaneous Imbibition as a Mechanism for Oil Recovery in Fractured Reservoirs. *Transport in Porous Media*, *101*(2), 299–331. https://doi.org/10.1007/s11242-013-0246-7

Annual Energy Outlook 2013—EIA. (n.d.). Retrieved from https://slidelegend.com/annual-energy-outlook-2013-eia_59dacf0b1723dd8efdef9314.html

Arogundade, O., & Sohrabi, M. (2012, January 1). *A Review of Recent Developments and Challenges in Shale Gas Recovery*. Presented at the SPE Saudi Arabia Section Technical Symposium and Exhibition. https://doi.org/10.2118/160869-MS

Barree, R. D., & Conway, M. W. (2005). Reply to Discussion of "Beyond Beta Factors: A Complete Model for Darcy, Forchheimer, and Trans-Forchheimer Flow in Porous Media." *Journal of Petroleum Technology*, *57*(08), 73–73. https://doi.org/10.2118/0805-0073-JPT

Belhaj, H. A., Agha, K. R., Nouri, A. M., Butt, S. D., Vaziri, H. F., & Islam, M. R. (2003, January 1). *Numerical Simulation of Non-Darcy Flow Utilizing the New Forchheimer's Diffusivity Equation*. Presented at the Middle East Oil Show. https://doi.org/10.2118/81499-MS

Berawala, Andersen, P. Ø., & Ursin, J. R. (2019). Controlling Parameters During Continuum Flow in Shale-Gas Production: A Fracture/Matrix-Modeling Approach. *SPE Journal*, *24*(03), 1378–1394. https://doi.org/10.2118/190843-PA

Berawala, & Østebø Andersen, P. (2019a, June 3). *Evaluation of Multicomponent Adsorption Kinetics for CO2 Enhanced Gas Recovery from Tight Shales*. Presented at the SPE Europec featured at 81st EAGE Conference and Exhibition. https://doi.org/10.2118/195536-MS

Berawala, & Østebø Andersen, P. (2019b, November 11). *Numerical Investigation of Non-Darcy Flow Regime Transitions in Shale Gas Production*. Presented at the Abu Dhabi International Petroleum Exhibition & Conference. https://doi.org/10.2118/197133-MS

Billemont, P., Coasne, B., & De Weireld, G. (2013). Adsorption of Carbon Dioxide, Methane, and Their Mixtures in Porous Carbons: Effect of Surface Chemistry, Water Content, and Pore Disorder. *Langmuir*, *29*(10), 3328–3338. https://doi.org/10.1021/la3048938

Bird, R. B. (2002). Transport phenomena. *Applied Mechanics Reviews*, *55*(1), R1–R4. https://doi.org/10.1115/1.1424298

Blasingame, T. A. (2008, January 1). *The Characteristic Flow Behavior of Low-Permeability Reservoir Systems*. Presented at the SPE Unconventional Reservoirs Conference. https://doi.org/10.2118/114168-MS

Busch, A., Alles, S., Gensterblum, Y., Prinz, D., Dewhurst, D. N., Raven, M. D., … Krooss, B. M. (2008). Carbon dioxide storage potential of shales. *International Journal of Greenhouse Gas Control*, *2*(3), 297–308. https://doi.org/10.1016/j.ijggc.2008.03.003

Bustin, A. M. M., Bustin, R. M., & Cui, X. (2008, January 1). *Importance of Fabric on the Production of Gas Shales*. Presented at the SPE Unconventional Reservoirs Conference.

https://doi.org/10.2118/114167-MS

Cao, P., Liu, J., & Leong, Y.-K. K. (2016). Combined impact of flow regimes and effective stress on the evolution of shale apparent permeability. *Journal of Unconventional Oil and Gas Resources*, *14*, 32–43. https://doi.org/10.1016/j.juogr.2016.01.004

Charoensuppanimit, P., Mohammad, S. A., & Gasem, K. A. M. (2016). Measurements and Modeling of Gas Adsorption on Shales. *Energy & Fuels*, *30*(3), 2309–2319. https://doi.org/10.1021/acs.energyfuels.5b02751

Chen, Z., Huan, G., & Ma, Y. (2006). *Computational methods for multiphase flows in porous media*. Philadelphia: Society for Industrial and Applied Mathematics.

Cipolla, C. L., Lolon, E. P., Erdle, J. C., & Rubin, B. (2010). Reservoir Modeling in Shale-Gas Reservoirs. *SPE Reservoir Evaluation & Engineering*, *13*(04), 638–653. https://doi.org/10.2118/125530-PA

Civan, F. (2010). Effective Correlation of Apparent Gas Permeability in Tight Porous Media. *Transport in Porous Media*, *82*(2), 375–384. https://doi.org/10.1007/s11242-009-9432-z

Civan, F., Rai, C. S., & Sondergeld, C. H. (2011). Shale-Gas Permeability and Diffusivity Inferred by Improved Formulation of Relevant Retention and Transport Mechanisms. *Transport in Porous Media*, *86*(3), 925–944. https://doi.org/10.1007/s11242-010-9665-x

Clarkson, C. R., Solano, N., Bustin, R. M., Bustin, A. M. M., Chalmers, G. R. L., He, L., … Blach, T. P. (2013). Pore structure characterization of North American shale gas reservoirs using USANS/SANS, gas adsorption, and mercury intrusion. *Fuel*, *103*, 606–616. https://doi.org/10.1016/j.fuel.2012.06.119

Darabi, H., Ettehad, A., Javadpour, F., & Sepehrnoori, K. (2012). Gas flow in ultra-tight shale strata. *Journal of Fluid Mechanics*, *710*, 641–658. https://doi.org/10.1017/jfm.2012.424

Davies, J. P., & Davies, D. K. (1999, January 1). *Stress-Dependent Permeability: Characterization and Modeling*. Presented at the SPE Annual Technical Conference and Exhibition. https://doi.org/10.2118/56813-MS

Davis, R. A. (1992). *Depositional systems: An introduction to sedimentology and stratigraphy* (2nd ed). Englewood Cliffs, N.J: Prentice Hall.

Dong, Z., Holditch, S. A., & McVay, D. A. (2012). Resource Evaluation for Shale Gas Reservoirs. *SPE Hydraulic Fracturing Technology Conference*. Presented at the SPE Hydraulic Fracturing Technology Conference, The Woodlands, Texas, USA. https://doi.org/10.2118/152066-MS

Dreisbach, F., Staudt, R., & Keller, J. U. (1999). High Pressure Adsorption Data of Methane, Nitrogen, Carbon Dioxide and their Binary and Ternary Mixtures on Activated Carbon. *Adsorption*, *5*(3), 215–227. https://doi.org/10.1023/A:1008914703884

Edwards, R. W. J., Celia, M. A., Bandilla, K. W., Doster, F., & Kanno, C. M. (2015). A Model To Estimate Carbon Dioxide Injectivity and Storage Capacity for Geological Sequestration in Shale Gas Wells. *Environmental Science & Technology*, *49*(15), 9222–9229. https://doi.org/10.1021/acs.est.5b01982

Fathi, E., & Akkutlu, I. Y. (2014). Multi-component gas transport and adsorption effects during CO_2 injection and enhanced shale gas recovery. *International Journal of Coal Geology*, *123*, 52–61. https://doi.org/10.1016/j.coal.2013.07.021

Faulkner, D. R., & Rutter, E. H. (1998). The gas permeability of clay-bearing fault gouge at 20°C. *Geological Society, London, Special Publications*, *147*(1), 147–156. https://doi.org/10.1144/GSL.SP.1998.147.01.10

Florence, F. A., Rushing, J., Newsham, K. E., & Blasingame, T. A. (2007, January 1). *Improved Permeability Prediction Relations for Low Permeability Sands*. Presented at the Rocky Mountain Oil & Gas Technology Symposium. https://doi.org/10.2118/107954-MS

Freeze, R. A., & Cherry, J. A. (1979). *Groundwater*. Englewood Cliffs, N.J: Prentice-Hall.

Ghanbarnezhad Moghanloo, R., & Javadpour, F. (2014). Applying Method of Characteristics

to Determine Pressure Distribution in 1D Shale-Gas Samples. *SPE Journal*, *19*(03), 361–372. https://doi.org/10.2118/168218-PA

Godec, M., Koperna, G., Petrusak, R., & Oudinot, A. (2013). Potential for enhanced gas recovery and CO2 storage in the Marcellus Shale in the Eastern United States. *International Journal of Coal Geology*, *118*, 95–104. https://doi.org/10.1016/j.coal.2013.05.007

Godec, M., Koperna, G., Petrusak, R., & Oudinot, A. (2014). Enhanced Gas Recovery and CO2 Storage in Gas Shales: A Summary Review of its Status and Potential. *Energy Procedia*, *63*, 5849–5857. https://doi.org/10.1016/j.egypro.2014.11.618

Haghshenas, B., Clarkson, C. R., & Chen, S. (2013, November 5). *Multi-Porosity Multi-Permeability Models for Shale Gas Reservoirs*. Presented at the SPE Unconventional Resources Conference Canada. https://doi.org/10.2118/167220-MS

Hagoort, J. (2004). Non-Darcy Flow Near Hydraulically Fractured Wells. *SPE Journal*, *9*(02), 180–185. https://doi.org/10.2118/80419-PA

He, W., Lv, W., & Dickerson, J. H. (2014). Gas Diffusion Mechanisms and Models. In W. He, W. Lv, & J. Dickerson (Eds.), *Gas Transport in Solid Oxide Fuel Cells* (pp. 9–17). https://doi.org/10.1007/978-3-319-09737-4_2

Heller, R., & Zoback, M. (2014). Adsorption of methane and carbon dioxide on gas shale and pure mineral samples. *Journal of Unconventional Oil and Gas Resources*, *8*, 14–24. https://doi.org/10.1016/j.juogr.2014.06.001

Hellmann, J. R., Scheetz, B. E., Luscher, W. G., Hartwich, D. G., & Koseski, R. P. (2014). *Proppants for shale gas and oil recovery: Engineering ceramics for stimulation of unconventional energy resources*.

Hill, D. G., & Nelson, C. R. (2000). Gas productive fractured shales: An overview and update. *Gas Tips*, *6*(3), 4–13.

Ho, C. K., & Webb, S. W. (Eds.). (2006). *Gas transport in porous media*. Dordrecht: Springer.

Holt, J. K. (2006). Fast Mass Transport Through Sub-2-Nanometer Carbon Nanotubes. *Science*, *312*(5776), 1034–1037. https://doi.org/10.1126/science.1126298

Huang, J., & Ghassemi, A. (2015). A poroelastic model for evolution of fractured reservoirs during gas production. *Journal of Petroleum Science and Engineering*, *135*, 626–644. https://doi.org/10.1016/j.petrol.2015.10.007

Javadpour, F. (2009). Nanopores and Apparent Permeability of Gas Flow in Mudrocks (Shales and Siltstone). *Journal of Canadian Petroleum Technology*, *48*(08), 16–21. https://doi.org/10.2118/09-08-16-DA

Jiang, J., & Yang, J. (2018). Coupled fluid flow and geomechanics modeling of stress-sensitive production behavior in fractured shale gas reservoirs. *International Journal of Rock Mechanics and Mining Sciences*, *101*, 1–12. https://doi.org/10.1016/j.ijrmms.2017.11.003

Jones, S. C. (1987, January 1). *Using the Inertial Coefficient, B, To Characterize Heterogeneity in Reservoir Rock*. Presented at the SPE Annual Technical Conference and Exhibition. https://doi.org/10.2118/16949-MS

Kang, S. M., Fathi, E., Ambrose, R. J., Akkutlu, I. Y., & Sigal, R. F. (2011). Carbon Dioxide Storage Capacity of Organic-Rich Shales. *SPE Journal*, *16*(04), 842–855. https://doi.org/10.2118/134583-PA

Karniadakis, G., Beşkök, A., & Aluru, N. R. (2005). *Microflows and nanoflows: Fundamentals and simulation*. New York, NY: Springer.

Kim, T. H., Cho, J., & Lee, K. S. (2017). *Evaluation of CO2 injection in shale gas reservoirs with multi-component transport and geomechanical effects*. https://doi.org/10.1016/j.apenergy.2017.01.047

Klinkenberg, L. J. (1941, January 1). *The Permeability Of Porous Media To Liquids And Gases*. Presented at the Drilling and Production Practice. Retrieved from

https://www.onepetro.org/conference-paper/API-41-200

Knudsen, M. (1909). Die Gesetze der Molekularströmung und der inneren Reibungsströmung der Gase durch Röhren. *Annalen der Physik*, *333*(1), 75–130. https://doi.org/10.1002/andp.19093330106

Kurniawan, Y., Bhatia, S. K., & Rudolph, V. (2006). Simulation of binary mixture adsorption of methane and CO2 at supercritical conditions in carbons. *AIChE Journal*, *52*(3), 957–967. https://doi.org/10.1002/aic.10687

Lake, L. W., Fanchi, J. R., & Society of Petroleum Engineers (U.S.) (Eds.). (2006). *Petroleum engineering handbook*. Richardson, TX: Society of Petroleum Engineers.

Li, D., & Engler, T. W. (2001, January 1). *Literature Review on Correlations of the Non-Darcy Coefficient*. Presented at the SPE Permian Basin Oil and Gas Recovery Conference. https://doi.org/10.2118/70015-MS

Lin, W., Li, X., Yang, Z., Lin, L., Xiong, S., Wang, Z., … Xiao, Q. (2018). A NEW IMPROVED THRESHOLD SEGMENTATION METHOD FOR SCANNING IMAGES OF RESERVOIR ROCKS CONSIDERING PORE FRACTAL CHARACTERISTICS. *Fractals*, *26*(02), 1840003. https://doi.org/10.1142/S0218348X18400030

Ling, K., He, J., Wu, X., & Shen, Z. (2013, March 26). *Determining Coefficient of Quadratic Term in Forchheimer Equation*. Presented at the International Petroleum Technology Conference. https://doi.org/10.2523/IPTC-16582-MS

Lu, X. C., Li, F. C., & Watson, A. T. (1995). Adsorption studies of natural gas storage in Devonian shales. *SPE Formation Evaluation*, *10*(2). https://doi.org/10.2118/26632-PA

Majumder, M., Chopra, N., Andrews, R., & Hinds, B. (2005). Erratum: Nanoscale hydrodynamics: Enhanced flow in carbon nanotubes. *Nature*, *438*(7070), 930–930. https://doi.org/10.1038/438930b

Masel, R. I. (1996). *Principles of adsorption and reaction on solid surfaces*. New York: Wiley.

Mengal, S. A., & Wattenbarger, R. A. (2011). Accounting for adsorbed gas in shale gas reservoirs. *SPE Middle East Oil and Gas Show and Conference*. Society of Petroleum Engineers.

Moridis, G. J., Blasingame, T. A., & Freeman, C. M. (2010, January 1). *Analysis of Mechanisms of Flow in Fractured Tight-Gas and Shale-Gas Reservoirs*. Presented at the SPE Latin American and Caribbean Petroleum Engineering Conference. https://doi.org/10.2118/139250-MS

Mustapha, H., de Langavant, L., & Giddins, M. A. (2015). Darcy and non-Darcy Flows in Fractured Gas Reservoirs. *SPE Reservoir Characterisation and Simulation Conference and Exhibition*. Presented at the SPE Reservoir Characterisation and Simulation Conference and Exhibition, Abu Dhabi, UAE. https://doi.org/10.2118/175596-MS

Nergård, K. (2018). *Investigation of Geomechanical Effects and Other Controlling Parameters on Shale Gas Production*.

Newsham, K. E., & Rushing, J. A. (2001). An Integrated Work-Flow Model to Characterize Unconventional Gas Resources: Part I - Geological Assessment and Petrophysical Evaluation. *SPE Annual Technical Conference and Exhibition*. Presented at the SPE Annual Technical Conference and Exhibition, New Orleans, Louisiana. https://doi.org/10.2118/71351-MS

Nuttall, B., & Daugherty, S. (2012). *Predicting Cumulative Production of Devonian Shale Gas Wells from Early Well Performance Data, Appalachian Basin of Eastern Kentucky. Kentucky Geological Survey*.

Ōtani, J., & Obara, Y. (Eds.). (2004). *X-ray CT for geomaterials: Soils, concrete, rocks: proceedings of the International Workshop on X-Ray CT for Geomaterials: GEOX2003: 6-7 November, 2003, Kumamoto, Japan*. Lisse, the Netherlands ; Exton, Pa: A.A. Balkema.

Ottiger, S., Pini, R., Storti, G., & Mazzotti, M. (2008). Competitive adsorption equilibria of CO2 and CH4 on a dry coal. *Adsorption*, *14*(4–5), 539–556. https://doi.org/10.1007/s10450-008-9114-0

Raghavan, R., & Chin, L. Y. (2002, January 1). *Productivity Changes in Reservoirs With Stress-Dependent Permeability*. Presented at the SPE Annual Technical Conference and Exhibition. https://doi.org/10.2118/77535-MS

Raghavan, R., & Chin, L. Y. (2004). Productivity Changes in Reservoirs With Stress-Dependent Permeability. *SPE Reservoir Evaluation & Engineering*, *7*(04), 308–315. https://doi.org/10.2118/88870-PA

Roy, S., Raju, R., Chuang, H. F., Cruden, B. A., & Meyyappan, M. (2003). Modeling gas flow through microchannels and nanopores. *Journal of Applied Physics*, *93*(8), 4870–4879. https://doi.org/10.1063/1.1559936

Rutqvist, J., Wu, Y.-S., Tsang, C.-F., & Bodvarsson, G. (2002). A modeling approach for analysis of coupled multiphase fluid flow, heat transfer, and deformation in fractured porous rock. *International Journal of Rock Mechanics and Mining Sciences*, *39*(4), 429–442. https://doi.org/10.1016/S1365-1609(02)00022-9

Sakhaee-pour, A., & Bryant, S. L. (2011). Gas Permeability of Shale. *SPE Annual Technical Conference and Exhibition*. Presented at the SPE Annual Technical Conference and Exhibition, Denver, Colorado, USA. https://doi.org/10.2118/146944-MS

Sakhaee-Pour, A., & Li, W. (2016). Fractal dimensions of shale. *Journal of Natural Gas Science and Engineering*, *30*, 578–582. https://doi.org/10.1016/j.jngse.2016.02.044

Shabro, V., Torres-Verdin, C., & Javadpour, F. (2011, January 1). *Numerical Simulation of Shale-Gas Production: From Pore-Scale Modeling of Slip-Flow, Knudsen Diffusion, and Langmuir Desorption to Reservoir Modeling of Compressible Fluid*. Presented at the North American Unconventional Gas Conference and Exhibition. https://doi.org/10.2118/144355-MS

Sherifa, C., & Reza, B. (2018). Carbon Dioxide Utilization and Sequestration in Kerogen Nanopores. *Carbon Capture, Utilization and Sequestration*. https://doi.org/10.5772/intechopen.78235

Sherman, F. S. (1969). The Transition From Continuum to Molecular Flow. *Annual Review of Fluid Mechanics*, *1*(1), 317–340. https://doi.org/10.1146/annurev.fl.01.010169.001533

Soeder, D. J. (1988). Porosity and Permeability of Eastern Devonian Gas Shale. *SPE Formation Evaluation*, *3*(01), 116–124. https://doi.org/10.2118/15213-PA

Sun, Hai, Yao, J., Cao, Y., Fan, D., & Zhang, L. (2017). Characterization of gas transport behaviors in shale gas and tight gas reservoirs by digital rock analysis. *International Journal of Heat and Mass Transfer*, *104*, 227–239. https://doi.org/10.1016/j.ijheatmasstransfer.2016.07.083

Sun, Hao, Chawathe, A., Hoteit, H., Shi, X., & Li, L. (2015). Understanding Shale Gas Flow Behavior Using Numerical Simulation. *SPE Journal*, *20*(01), 142–154. https://doi.org/10.2118/167753-PA

Wang, F. P., & Reed, R. M. (2009, January 1). *Pore Networks and Fluid Flow in Gas Shales*. Presented at the SPE Annual Technical Conference and Exhibition. https://doi.org/10.2118/124253-MS

Wang, H., & Marongiu-Porcu, M. (2015). Impact of Shale-Gas Apparent Permeability on Production: Combined Effects of Non-Darcy Flow/Gas-Slippage, Desorption, and Geomechanics. *SPE Reservoir Evaluation & Engineering*, *18*(04), 495–507. https://doi.org/10.2118/173196-PA

Wang, J., Luo, H., Liu, H., Cao, F., Li, Z., & Sepehrnoori, K. (2017). An Integrative Model To Simulate Gas Transport and Production Coupled With Gas Adsorption, Non-Darcy Flow, Surface Diffusion, and Stress Dependence in Organic-Shale Reservoirs. *SPE Journal*, *22*(01),

244–264. https://doi.org/10.2118/174996-PA

Weijermars, R. (2013). Economic appraisal of shale gas plays in Continental Europe. *Applied Energy*, *106*, 100–115. https://doi.org/10.1016/j.apenergy.2013.01.025

Weniger, P., Kalkreuth, W., Busch, A., & Krooss, B. M. (2010). High-pressure methane and carbon dioxide sorption on coal and shale samples from the Paraná Basin, Brazil. *International Journal of Coal Geology*, *84*(3), 190–205. https://doi.org/10.1016/j.coal.2010.08.003

Winterfeld, P. H., & Wu, Y.-S. (2011, January 1). *Parallel Simulation of CO2 Sequestration with Rock Deformation in Saline Aquifers*. Presented at the SPE Reservoir Simulation Symposium. https://doi.org/10.2118/141514-MS

Wu, K., Li, X., Guo, C., Wang, C., & Chen, Z. (2016). A Unified Model for Gas Transfer in Nanopores of Shale-Gas Reservoirs: Coupling Pore Diffusion and Surface Diffusion. *SPE Journal*, *21*(05), 1,583-1,611. https://doi.org/10.2118/2014-1921039-PA

Wu, Y.-S., Li, J., Ding, D., Wang, C., & Di, Y. (2014). A Generalized Framework Model for the Simulation of Gas Production in Unconventional Gas Reservoirs. *SPE Journal*, *19*(05), 845–857. https://doi.org/10.2118/163609-PA

Wu, Y.-S., Pruess, K., & Persoff, peter. (1998). Gas Flow in Porous Media With Klinkenberg Effects. *Transport in Porous Media*, *32*(1), 117–137. https://doi.org/10.1023/A:1006535211684

Wua, K., Li, X., Guo, C., & Chen, Z. (2015). Adsorbed Gas Surface Diffusion and Bulk Gas Transport in Nanopores of Shale Reservoirs with Real Gas Effect-Adsorption-Mechanical Coupling. *SPE Reservoir Simulation Symposium*. Presented at the SPE Reservoir Simulation Symposium, Houston, Texas, USA. https://doi.org/10.2118/173201-MS

Xiong, X., Devegowda, D., Michel Villazon, G. G., Sigal, R. F., & Civan, F. (2012). A Fully-Coupled Free and Adsorptive Phase Transport Model for Shale Gas Reservoirs Including Non-Darcy Flow Effects. *SPE Annual Technical Conference and Exhibition*. Presented at the SPE Annual Technical Conference and Exhibition, San Antonio, Texas, USA. https://doi.org/10.2118/159758-MS

Yi, J., Akkutlu, I. Y., Karacan, C. Ö., & Clarkson, C. R. (2009). *Gas sorption and transport in coals: A poroelastic medium approach*. https://doi.org/10.1016/j.coal.2008.09.016

Yu, W., & Sepehrnoori, K. (2014). Simulation of gas desorption and geomechanics effects for unconventional gas reservoirs. *Fuel*, *116*, 455–464. https://doi.org/10.1016/j.fuel.2013.08.032

Yu, W., Sepehrnoori, K., & Patzek, T. W. (2016). Modeling Gas Adsorption in Marcellus Shale With Langmuir and BET Isotherms. *SPE Journal*, *21*(02), 589–600. https://doi.org/10.2118/170801-PA

Zeng, F., & Zhao, G. (2006, January 1). *Semi-Analytical Model for Reservoirs with Forchheimer's Non-Darcy Flow*. Presented at the SPE Gas Technology Symposium. https://doi.org/10.2118/100540-MS

Zhang, T., Ellis, G. S., Ruppel, S. C., Milliken, K., & Yang, R. (2012). Effect of organic-matter type and thermal maturity on methane adsorption in shale-gas systems. *Organic Geochemistry*, *47*, 120–131. https://doi.org/10.1016/j.orggeochem.2012.03.012

Zhang, Z. Y., & Yang, S. B. (2012). On the adsorption and desorption trend of shale gas. *Journal of Experimental Mechanics*, *27*(5), 492–497.

Ziarani, A. S., & Aguilera, R. (2012). Knudsen's Permeability Correction for Tight Porous Media. *Transport in Porous Media*, *91*(1), 239–260. https://doi.org/10.1007/s11242-011-9842-6

Zoback, M. D., & Kohli, A. H. (2019). *Unconventional Reservoir Geomechanics: Shale Gas, Tight Oil, and Induced Seismicity* (1st ed.). https://doi.org/10.1017/9781316091869

APPENDIX A -Initial and Current Gas in Place and Gas Recovery

The gas currently in place ($GCIP$) in kilogram is estimated on the base of the mass of gas adsorbed in the matrix ($Mass_1$), free gas in the fracture ($Mass_2$) and free gas in the matrix ($Mass_3$). These masses, considered over both sides of the fracture, and both analytically and numerically are evaluated.

$$Mass_1 = 2h \int_{x=0}^{L_x} \int_{y=0}^{L_y} (1 - \phi^m(P_t)) a_i(P_m(x,y), P_c(x,y)) \, dx \, dy =$$

$$2h \sum_{j=1}^{n_x} \sum_{k=1}^{n_y} (1 - \phi^m(P_t)) \hat{a}_i \left(P_m(x_j, y_k), P_c(x_j, y_k) \right) \Delta x \, \Delta y \qquad (60)$$

For calculation of GOIP , just there is methane in the matrix and for calculation of GCIP just the amount of methane is important in recovery formula. So we have :

$$Mass_1 = 2h \sum_{j=1}^{n_x} \sum_{k=1}^{n_y} (1 - \phi^m(P_t)) a_i \left(P_m(x_j, y_k) \right) \Delta x \, \Delta y$$

$$Mass_2 = \int_V \phi^f \, \rho_g \, dV = 2h \, \phi^f \int_{x=-2b}^{0} \int_{y=0}^{L_y} \rho_g \, dx \, dy \qquad (60)$$

$$= \phi^f \, \rho_{g,sc} b_g' \, h \int_{x=-2b}^{0} \int_{y=0}^{L_y} P_t(x,y) \, dx \, dy$$

$$= \phi^f \, \rho_{g,sc} b_g' \, h \int_{x=-2b}^{0} \int_{y=0}^{L_y} (P_m(x,y) + P_c(x,y)) \, dx \, dy$$

$$= \phi^f \, \rho_{g,sc} b_g' \, 2b \, h \sum_{k=1}^{n_y} P_t(y_k) \, \Delta y$$

$$= \phi^f \, \rho_{g,sc} b_g' \, 2b \, h \sum_{k=1}^{n_y} (P_m(y_k) + P_c(y_k)) \, \Delta y$$

For calculation of GOIP , just there is methane in fracture and for calculation of GCIP the amount of methane is important in recovery formula. So we have :

$$Mass_2 = \phi^f \, \rho_{g,sc} b_g' \, 2b \, h \sum_{k=1}^{n_y} (P_m(y_k)) \, \Delta y$$

$$Mass_3 = \int_V \phi^m \rho_g\, x_i\, dV = 2h \int\limits_{x=0}^{L_x}\int\limits_{y=0}^{L_y} \phi^m\, \rho_g\, dx\, dy$$

$$= 2h\; \rho_{g,sc} b'_g \int\limits_{x=0}^{L_x}\int\limits_{y=0}^{L_y} \phi^m\, P_t(x,y)\, dx\, dy$$

$$= 2h\; \rho_{g,sc} b'_g \sum_{k=1}^{n_y}\sum_{j=1}^{n_x} \phi^m\, P_t(x_j, y_k)\, \Delta x\, \Delta y$$

$$= 2h\; \rho_{g,sc} b'_g \sum_{j=1}^{n_x}\sum_{k=1}^{n_y} \phi^m\left(P_m(x_j, y_k)\right)\, \Delta x\, \Delta y$$

(61)

$GCIP = Mass_1 + Mass_2 + Mass_3$

For the gas originally in place, on the base of mass concentration of gas (mass per volume) as free gas in matrix and fracture and mass adsorbed by matrix we have:

$$GOIP = \int_V \phi\; \rho_g x_i + (1 - \phi^m)a_i\big(P_m(x,y), P_c(x,y)\big)\, dV\,|\,P_{t,init}$$

(62)

The above equation will be considered for both side of matrix. Now we calculate the free gas:

$$\rho_g(P_{t,0}) = \rho_{g,sc} b'_g\, P_{t,init}$$

(63)

The pore volume of free gas is as below:

$$\big(2\, b\, L_y\big)h\, \phi^f + \big(2\, L_x L_y\big)h\, \phi^m$$

(64)

Now the adsorbed gas amount in P_{init} with pressure unit (Pa) is as below:

$$\hat{a}_i\big(P_{m,init}, P_{c,init}\big) = \frac{a_i\big(P_{m,init}, P_{c,init}\big)}{\rho_{g,sc} b'_g} = \frac{a_i\big(P_{m,0}, P_{c,0} = 0\big)}{\rho_{g,sc} b'_g}$$

(65)

The adsorbed gas location is in the bulk volume of matrix as it is written in below:

$$\big(2\, L_x L_y\big)$$

(66)

The gas originally in place ($GOIP$) in kilogram could be estimated by the concept of identical pressure in all parts (matrix and fracture) is equal to total initial pressure ($P_{t,init}$).

$$GOIP = GCIP\,(P_{init}) = \big[\big(2\, b\, L_y\big)\phi^f + \big(2\, L_x L_y\big)\phi^m\big]\rho_{g,sc} b'_g\, h\, P_{t,init} +$$
$$\big(2\, L_x L_y\big)(1 - \phi^m)\, h\, \hat{a}_i\big(P_{m,init}, P_{c,init}\big)\rho_{g,sc} b'_g$$

(67)

$GOIP$ is also possible in the below form:

$$GOIP = GCIP(P_{init})$$
$$= \phi^f \rho_{g,sc} b'_g\, h\, \big(2\, b\, L_y\big)\left(P_{m,0}(y_k)\right)$$
$$+ \phi^m \rho_{g,sc} b'_g\, h\, \big(2\, L_x L_y\big)\left(P_{m,0}(x_j, y_k)\right)$$
$$+ \big(2\, L_x L_y\big)(1 - \phi^m)h\, \hat{a}_i\big(P_{m,init}, P_{c,init}\big)\rho_{g,sc} b'_g$$

(68)

We know that $2\, b$ is the average fracture width. The recovery factor RF is then calculated as below:

$$RF = 1 - \frac{GCIP}{GOIP} = 1 - \frac{GCIP}{GCIP(P_{t,init})}$$

(69)

The obtainable recovery factor RF_∞ is the amount of RF when the reservoir pressure reached uniformly the well pressure,

$$RF_\infty = 1 - \frac{GCIP(P_{t,well})}{GOIP} = 1 - \frac{GCIP(P_{t,well})}{GCIP(P_{t,init})} \tag{70}$$

So the fraction of obtainable recovery is determined by

$$RF_{ob} = \frac{RF}{RF_\infty} = \frac{GCIP(P_{t,init}) - GCIP}{GCIP(P_{t,init}) - GCIP(P_{t,well})} \tag{71}$$

By approximation of RF_∞ as a function of the well pressure, possible to consider only the contribution of matrix.

$$RF_\infty \approx 1 - \frac{\phi^m \rho_{g,sc} b'_g P_{t,well} + (1 - \phi^m) a_i(P_{m,well}, P_{c,well})}{\phi^m \rho_{g,sc} b'_g P_{t,init} + (1 - \phi^m) a_i(P_{m,init}, P_{c,init})}$$

$$= 1 - \frac{\phi^m P_{t,well} + (1 - \phi^m) \hat{a}_i(P_{m,well}, P_{c,well})}{\phi^m P_{t,init} + (1 - \phi^m) \hat{a}_i(P_{m,init}, P_{c,init})} \tag{72}$$

APPENDIX B-Operator Splitting

We solve the equations (55) and (56) using an operator-splitting approach identical to that defined in Andersen et al. (2014, 2015) and Andersen and Evje (2016): if we split the coupled system into three subsystems.

System One
Fracture Diffusion

The first subsystem contained fracture diffusion and flow in the $y - direction$.
So, set the $\partial_x p = 0$ and $\partial_t \hat{a}_i = 0$,

$$\phi^f \partial_t(p_i) = \frac{k^f}{\mu_g} \partial_y(p_i \partial_y (p_t)), \qquad (i = m, c) \; (x, y \in \Omega^f) \tag{73}$$

For matrix while adsorbed mass of CH4 and CH4 is kept constant and no difference in porosity.

$$\partial_t(\phi P_i + (1 - \phi) \hat{a}_i) = 0, \qquad\qquad (i = m, c) \; (x, y \in \Omega^m) \tag{74}$$

System Two
Fracture/Matrix Diffusion

The second system contained fracture/matrix diffusion and flow in the $x - direction$ and no desorption $\partial_t \hat{a}_i = 0$.

$$b \, \phi^f \, \partial_t(p_i) = \frac{k^m}{\mu_g} (p_i \, \partial_x(p_t))_{x=0,y} \quad (i = m, c) \; (x, y \in \Omega^f) \tag{75}$$

$$\partial_t(\phi P_i) = \frac{1}{\mu_g} \partial_x(k^m \partial_x(P_t) P_i) + \widehat{D}_i \, \partial_x(\phi \, \partial_x(P_i)) \; (i = m, c)$$

$$(x, y \in \Omega^m) \tag{76}$$

This system will be split into third subsystem where we just take into account diffusion of free gas with adsorbed mass kept fixed, and balance the adsorbed gas with free gas in the matrix. We apply the well-known Strang splitting approach where system a is solved during the time $\frac{\Delta T}{2}$ and system b is solved during the time ΔT, before the system a is solved for time $\frac{\Delta T}{2}$ again. ΔT is the so-called splitting timestep and small enough should be selected to allow the different systems to participate periodically enough to prepare relevant data regarding each other's solution procedure.

System Three
Sorption-porosity-pressure distribution

No flow is considered. It means that $\partial_x p = 0$ and $\partial_y p = 0$.

$b \, \phi^f \, \partial_t(p_i) = 0$,	$(i = m, c) \; (x, y \in \; \Omega^f)$	(77)

In the matrix the porosity and the adsorption is constant with the time.

$\partial_t(\phi \, P_i + (1 - \phi) \, \hat{a}_i \,) = 0$,	$(i = m, c) \; (x, y \in \; \Omega^m)$	(78)

No diffusive and advective flow will be considered, so. The masses of CO_2 and CH_4 are redistributed between free gas and adsorbed form to satisfy isotherm equilibrium during mass preservation. So, locally we need to adjust P_i , $\hat{a}_i(P_m(t), P_c(t))$ to be in equilibrium. To find the updated pressures P_m, P_c the conserved property is:

$M_m = \phi \; P_m + (1 - \phi) \, \hat{a}_m(P_m, P_c)$, $\qquad M_c = \phi \; P_c + (1 - \phi) \, \hat{a}_c(P_m, P_c)$		(79)

$P_{m,pre}$ and $P_{c,pre}$ evaluated at t_n before the transport steps, so we can evaluate M_{m_pre} and M_{c_pre} on the base of previous pressures like below:

$M_{m\_pre} = \phi(\, P_{t,pre}) \, P_{m,pre} + \big(1 - \phi(\, P_{t,pre})\big) \, \hat{a}_m\big(P_{m,pre}, P_{c,pre}\big)$,	(80)

$M_{c\_pre} = \phi(\, P_{t,pre}) \, P_{c,pre} + \big(1 - \phi(\, P_{t,pre})\big) \, \hat{a}_c\big(P_{m,pre}, P_{c,pre}\big)$,	(81)

Now we have previous methane and carbon dioxide conserved properties and there are no change in updated amounts of each component. $P_{m,new}$ and $P_{c,new}$ are evaluated at t_{n+1} after the transport steps, but the porosity and adsorption they have been constant. We note that the porosity is as a function of pressure in an isotherm equilibrium while preserving mass.

$M_m = \phi(\, P_{t,old}) \, P_{m,new} + \big(1 - \phi(\, P_{t,old})\big) \, \hat{a}_m\big(P_{m,old}, P_{c,old}\big)$,	(82)

$M_c = \phi(\, P_{t,old}) \, P_{c,new} + \big(1 - \phi(\, P_{t,old})\big) \, \hat{a}_c\big(P_{m,old}, P_{c,old}\big)$,	(83)

The values of M_m and M_c are known from the above calculation. So, we need to calculate the adjusted pressures $P_{m,adj}$ and $P_{c,adj}$ then we have:

$M_m = \phi(\, P_{t,adj}) \, P_{m,adj} + \big(1 - \phi(\, P_{t,adj})\big) \, \hat{a}_m\big(P_{m,adj}, P_{c,adj}\big)$,	(84)

$M_c = \phi(\, P_{t,adj}) \, P_{c,adj} + \big(1 - \phi(\, P_{t,adj})\big) \, \hat{a}_c\big(P_{m,adj}, P_{c,adj}\big)$,	(85)

To solve the above equations were defined in the following from:

$$P_{m,adj} = \frac{M_m}{\phi(\, P_{t,adj}) + \dfrac{\big(1 - \phi(\, P_{t,adj})\big)\hat{a}_m\big(P_{m,adj}, P_{c,adj}\big)}{P_{m,adj}}}$$	(86)

$$P_{c,adj} = \frac{M_c}{\phi(P_{t,adj}) + \dfrac{(1 - \phi(P_{t,adj}))\hat{a}_c(P_{m,adj}, P_{c,adj})}{P_{c,adj}}} \tag{87}$$

So we have two unknown pressures and two equations, after solve of the above equations, we know the amount of porosity, adsorbed amount of mass, free gas pressure, and then possible to calculate apparent permeability, this equation should be solved by iteration simultaneously at once for every cell in in x direction.

APPENDIX C-Discretization

We assume that y-axis is discretized into $k = 1 : N_y$ cells and the matrix into $j=1: N_x$ cells.

Fracture Diffusion

In this part we just consider the fracture and no changes in the matrix. The half width is b And for a given cell k b_k is constant. The conserved property is P_t, which consolidated over the grid cells and from (73) we have:

$$\frac{\phi^f([P_i]_k^{n+1} - [P_i]_k^n)}{\Delta t} = \frac{K^f}{\mu} \frac{[P_i]_{k+\frac{1}{2},j}^n \, \partial_y \, [P_t]_{k+\frac{1}{2},j}^n - [P_i]_{k-\frac{1}{2},j}^n \, \partial_y \, [P_t]_{k-\frac{1}{2},j}^n}{\Delta y} \tag{88}$$

The flux is selected by an upstream system, but it is needed to take into account the flow direction is from fracture top most toward well and the pressure decreasing so we have:

$$[P_i]_{k+\frac{1}{2},j}^n \, \partial_y \, [P_t]_{k+\frac{1}{2},j}^n = [P_i]_{k+\frac{1}{2},j}^n \left([P_t]_{k,j}^n - [P_t]_{k+1,j}^n\right) \qquad (i = m, c) \tag{89}$$

$$[P_i]_{k+\frac{1}{2},j}^n = [P_i]_{k,j}^n \quad , \text{ if } \left([P_t]_{k,j}^n > [P_t]_{k+1,j}^n\right),$$

$$[P_i]_{k+\frac{1}{2},j}^n = [P_i]_{k,j}^n \quad , \text{ if } \left([P_t]_{k+1,j}^n > [P_t]_{k,j}^n\right),$$

We know that on the base of our assumptions porosity of fracture is constant over time step and could be computed by using the pressure at previous time step, then we have:

$$\frac{\phi^f([P_i]_k^{n+1} - [P_i]_k^n)}{\Delta t} = \frac{K^f}{\mu} \frac{\left([P_i]^n \, \partial_y \, [P_t]^n\right)_{k+\frac{1}{2},j} - \left([P_i]^n \, \partial_y \, [P_t]^n\right)_{k-\frac{1}{2},j}}{\Delta y} \tag{90}$$

And then we have :

$$[P_i]_k^{n+1} = \frac{\Delta t \, K^f \left([P_i]_{k+\frac{1}{2},j}^n \, \partial_y \, [P_t]_{k+\frac{1}{2},j}^n - [P_i]_{k-\frac{1}{2},j}^n \, \partial_y \, [P_t]_{k-\frac{1}{2},j}^n\right)}{\phi^f \, \mu \, \Delta y} + [P_i]_k^n \tag{91}$$

At the fracture boundaries, we set:

$$P_0 = 0, \qquad \left(P_i \, \partial_y \, P_t \right)_{N_y+\frac{1}{2}} = 0 \tag{92}$$

Fracture/Matrix Diffusion

The equation (76) for matrix formula can be discretized with no desorption, so we set $\partial_t \, \hat{a}_i = 0$ and then for the central cell in the matrix we have:

$$
\frac{\left([P_i]_j^{n+1}\phi_j^{n+1} - [P_i]_j^n \, \phi_j^{\,n} \right)}{\Delta t}
$$

$$
= \frac{\left(\dfrac{k^m}{\mu}\right)_{j+\frac{1}{2},k} [P_i]_{j+\frac{1}{2},k}^n \, \partial_x \, [P_t]_{j+\frac{1}{2},k}^n - \left(\dfrac{k^m}{\mu}\right)_{j-\frac{1}{2},k} [P_i]_{j-\frac{1}{2},k}^n \, \partial_x \, [P_t]_{j-\frac{1}{2},k}^n}{\Delta x}
$$

$$
+ \frac{\widehat{D}_i \left[(\phi)_{j+\frac{1}{2},k} \, \partial_x \, [P_i]_{j+\frac{1}{2},k}^n - (\phi)_{j-\frac{1}{2},k} \, \partial_x \, [P_i]_{j-\frac{1}{2},k}^n \right]}{\Delta x} , \qquad (i = m, c) \tag{93}
$$

With the advective flux is described by an upstream system:

$$
(k^m \, [P_i] \, \partial_x \, [P_t])_{j+\frac{1}{2},k} = \frac{2}{\left(\dfrac{1}{k_{j+1,k}^m}\right) + \left(\dfrac{1}{k_{j,k}^m}\right)} [P_i]_{j+\frac{1}{2},k}^n \frac{[P_t]_{j+1,k}^n - [P_t]_{j,k}^n}{\Delta x}, \quad (i = m, c), \tag{94}
$$

$$
[P_i]_{j+\frac{1}{2},k}^n = [P_i]_{j+1,k}^n, \text{ if } \left([P_t]_{j+1,k}^n > [P_t]_{j,k}^n\right),
$$

$$
[P_i]_{j+\frac{1}{2},k}^n = [P_i]_{j,k}^n, \text{ if } \left([P_t]_{j,k}^n > [P_t]_{j+1,k}^n\right),
$$

And the diffusive fluxes described by:

$$
\widehat{D}_i (\phi)_{j+\frac{1}{2},k} \, \partial_x \, [P_i]_{j+\frac{1}{2},k}^n = \widehat{D}_i \frac{\phi_{j+1,k} + \phi_{j,k}}{2} \frac{[P_i]_{j+1,k}^n - [P_i]_{j,k}^n}{\Delta x}, \qquad (i = m, c). \tag{95}
$$

The diffusive flux at the inlet and both advective and diffusive fluxes at matrix outer boundary that is $x = L_x$ are set to zero.

$$
\left(\frac{K^m}{\mu} \, P_i \, \partial_x \, P_t \right)_{N_x+\frac{1}{2}} = 0 , \quad \partial_x \, [P_i]_{N_x+\frac{1}{2}}^n = 0 \tag{96}
$$

At the fracture/matrix interface for fracture equation we have:

$$
\frac{b_k \phi^f ([P_i]_0^{n+1} - [P_i]_0^n)}{\Delta t} = \left(\frac{K^m}{\mu} \, P_i \, \partial_x \, P_t \right)_{j=\frac{3}{2},k} \qquad (i = m, c) \, (x, y \in \Omega^f) \tag{97}
$$

$$
\frac{([P_i]_1^{n+1} - [P_i]_1^n)}{\Delta t} = \frac{\dfrac{k^m}{\mu} (P_i \, \partial_x \, P_t)_{j=\frac{3}{2},k}}{b_k \phi^f \Delta x} \tag{98}
$$

$$(i = m, c)(x, y \in \Omega^m)$$

The fracture/matrix flux term at the interface defined by

$$\left(\frac{k^m}{\mu} \, P_i \, \partial_x \, P_t\right)_{j=\frac{3}{2},k} = \frac{1}{\mu} \frac{2}{\left(\frac{1}{k_1^m}\right) + \left(\frac{1}{k_2^m}\right)} [P_i]^n_{j=\frac{3}{2},k} \frac{[P_t]_2 - [P_t]_1}{\left(\frac{\Delta x}{2}\right)} \quad (99)$$

$$[P_i]^n_{j=\frac{3}{2},k} = [P_i]^n_{j=2,k}, \text{if } \left([P_t]^n_{j=2,k} > [P_t]^n_{j=1,k}\right),$$

$$[P_i]^n_{j=\frac{3}{2},k} = [P_i]^n_{1,k}, \text{ if } \left([P_t]^n_{j=1,k} > [P_t]^n_{j=2,k}\right),$$

Same as the central fluxes, except that the pressure gradient at the fracture interface is given and not in the fracture center. Ultimately, the flux is set to be zero at the outer boundary of the matrix.

$$\left(\frac{k^m}{\mu} \, P_i \, \partial_x \, P_t\right)_{j=N_x+\frac{1}{2},k} = 0 \, , \quad (100)$$

Stability

For stability, we need the pressure with no fluctuation because it is assumed that behave in a diffusive trend and drive mass changes. If by selecting too large timestep, too much gas is transported, we may observe fluctuations in pressure profiles. To check the stability we assume three adjacent cells $j-1$, j, and $j+1$ in the matrix. At each computation, we need to assure that the pressure change in cell j to not be more in a timestep than one-half of the maximum difference in pressure between cell j and its neighbor cells. This method allows us to select the higher timesteps consequently.

$$\left|[P]_j^{n+1} - [P]_j^n\right| \le \frac{1}{2} max \left(\left|[P]_{j+1} - [P]_j\right|, \left|[P]_j - [P]_{j-1}\right|\right), \quad (101)$$

And also for checking the stability in fracture we have:

$$\left|[P]_k^{n+1} - [P]_k^n\right| \le \frac{1}{2} max \left(\left|[P]_{k+1} - [P]_k\right|, \left|[P]_k - [P]_{k-1}\right|\right), \quad (102)$$